Published online in Int. J. Numer. Meth. Biomed. Engng.. DOI: 10.1002/cnm.2918

Benchmark problems for numerical treatment of backflow at open boundaries

C. Bertoglio[1,11*†], A. Caiazzo[2†], Y. Bazilevs[3], M. Braack[4], M. Esmaily[5,12], V. Gravemeier[8,10], A. Marsden[9], O. Pironneau[6], I.E. Vignon-Clementel[6,7], W.A. Wall[8]

[1] *Center for Mathematical Modeling, Universidad de Chile, Santiago, Chile*
[2] *Weierstrass Institute for Applied Analysis and Stochastics (WIAS) Leibniz Institute in Forschungsverbund Berlin e.V., Berlin, Germany*
[3] *Department of Structural Engineering, University of California, San Diego, USA*
[4] *Research Group for Applied Mathematics, Christian-Albrechts-Universität, Kiel, Germany*
[5] *Sibley School of Mechanical and Aerospace Engineering, Cornell University, Ithaca, NY 14850, USA*
[6] *Laboratoire Jacques-Louis Lions, University Pierre et Marie Curie, Paris, France*
[7] *REO Project team, INRIA, Paris, France*
[8] *Institute for Computational Mechanics, Technical University of Munich, Garching b. München, Germany*
[9] *Cardiovascular Biomechanics Computational Lab, Stanford University, CA, USA*
[10] *AdCo Engineering^{GW} GmbH, Garching b. München, Germany*
[11] *Johann Bernoulli Institute, University of Groningen, Groningen, The Netherlands*
[12] *Center for Turbulence Research, Stanford University, CA, USA*

SUMMARY

In computational fluid dynamics, incoming velocity at open boundaries, or *backflow*, often yields to unphysical instabilities already for moderate Reynolds numbers. Several treatments to overcome these backflow instabilities have been proposed in the literature. However, these approaches have not yet been compared in detail in terms of accuracy in different physiological regimes, in particular due to the difficulty to generate stable reference solutions apart from analytical forms. In this work, we present a set of benchmark problems in order to compare different methods in different backflow regimes (with a full reversal flow and with propagating vortices after a stenosis). The examples are implemented in FreeFem++ and the source code is openly available, making them a solid basis for future method developments.

Received ...

KEY WORDS: Navier-Stokes Equations, backflow stabilization, benchmarking, blood flows, respiratory flows

1. INTRODUCTION

In computational fluid dynamics, open boundaries denote the boundaries where the velocity is not prescribed, using a natural boundary condition instead. These boundary conditions are very relevant in physiological flow simulations, e.g., when modeling the cardiovascular and the respiratory systems, where accurate velocity data are rarely available on all boundaries and/or only pressures and averaged flow quantities may be measured or computed via a reduced model of the rest of the system. Moreover, the need of setting the right boundary condition on open

*Correspondence to: Cristóbal Bertoglio, Nijenborgh 9, 9747 AG Groningen, The Netherlands E-mail: c.a.bertoglio@rug.nl
†These authors contributed equally to this work

boundaries becomes more important when the computational domains are obtained truncating the geometry in order to reduce the computational cost by focusing the analysis on a region of interest, see examples in Figure 1.

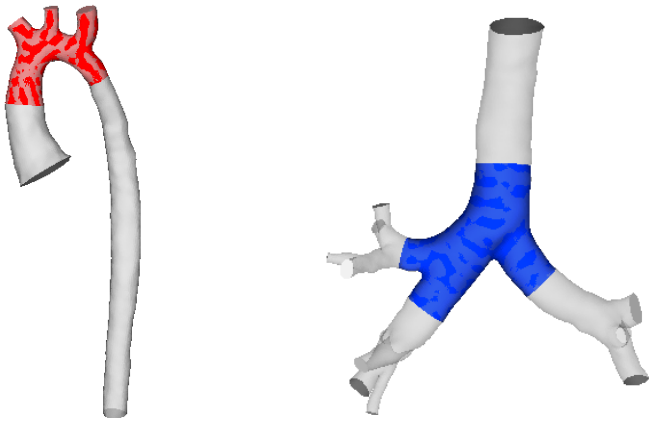

Figure 1. Illustration of the truncation of the computational domain (colored) from the originally segmented medical image (grey). Left: Aorta. Right: Airways.

Due to the periodicity of the physiology in the cardiovascular and respiratory systems, depending on the physical regime and on the considered geometry, flow reversal might appear at open boundaries. This situation is known in the literature as *backflow* and one may distinguish between two patterns:

1. Full backflow, i.e., when the flow enters the computational domain at each point of the open boundary. In blood flow, this situation can be encountered for example in the vessels branching from the aorta in diastole. In respiratory flow, flow rate reverses between inspiration and expiration.
2. Local backflow, i.e. when flow re-circulates through the open boundary due to the propagation of vortex shedding, as it might be the case when the computational domain contains curved tubes or stenoses (reduction of cross sectional area).

From the point of view of the analysis, general well posedness results are rarely available for the incompressible Navier-Stokes Equations in presence of reversed flow at the open boundaries. This is consistent with the fact that, in numerical practice, it is well known that numerical simulations might suffer of instabilities when backflow appears.

Up to date, several proposals to overcome this issue have appeared in the literature (see Section 3), mainly consisting in modifying the natural boundary conditions in order to enhance the overall stability. However, to our best knowledge, the different backflow treatments have neither yet been compared in detail in terms of accuracy (i.e., with respect to a reference solution) nor considering different physiological regimes and the different backflow patterns described above. To some extent, this is also due to the difficulty of generating stable reference solutions with arbitrary backflow. Hence, the main goal of this work is to formulate a set of benchmark problems, relevant for both physiological blood and respiratory flow regimes, and to assess the performance of several backflow stabilization methods.

Benchmark problems are important tools for evaluation of numerical schemes with respect to accuracy and efficiency. For the numerical simulation of incompressible fluids via Navier-Stokes Equations, well established benchmarks have been proposed, such as the "Flow around a cylinder" [35], the "Driven-cavity problems" in 2D [21] and 3D [9, 25] or the "Thermally-driven Flows at Low Mach Number" [28].

However, until now benchmark problems in fluid mechanics with the focus on appropriate open boundary treatment, i.e. on boundary conditions which are not of Dirichlet-type are

DOI: 10.1002/cnm.2918

still missing. Therefore this work represents an important contribution for the field of computational fluid dynamics, also beyond the simulation of physiological flows.

In order to construct relevant examples of numerical simulations affected by backflow instabilities, and, at the same time, to allow for an easier reproducibility of the test-cases and of the results (an essential requirement of benchmarking), we focus on two-dimensional problems. Although 2D models cannot fully reproduce the complexity arising in 3D flows (e.g., the arise of Dean flow in curved pipes), we note that good agreements between 2D and 3D test-cases, concerning the issues related to backflow instabilities, have been already reported, e.g., in [6].

Firstly, we consider a reverse flow in a channel, for which the reference solution is generated by solving the incompressible Navier-Stokes Equations using a Dirichlet boundary condition for the inflow boundary. Then, the benchmark problem is based on the same domain but imposing a Neumann boundary condition on the inflow boundary, computed from the reference velocity and pressure solutions.

Secondly, we consider a channel with a stenosis, in which a vortex shedding arises, producing recirculation regions at the open boundary. In this case, a reference solution is generated considering a long channel so that multiple vortices propagate downstream before reaching the open boundary. Then, the benchmark problem is defined considering a shorter channel and imposing on the open boundary a natural boundary condition based on the traction computed for the longer geometry.

In this manuscript, we focus on finite element methods for solving the benchmark problems, as it has been used to discretize all the considered backflow stabilization methods. However, it is worth noticing that the proposed benchmarking procedures are independent of the adopted spatio-temporal discretization, since they are defined at the continuous level.

The rest of the paper is organized as follows. In Section 2 we describe the natural boundary conditions and derive the source of energy instabilities. In Section 3 the backflow stabilization methods are reviewed. The benchmarks and the numerical results are presented in Sections 4 and 5, discussing the outcome in Section 6.

2. INCOMPRESSIBLE NAVIER-STOKES WITH OPEN BOUNDARIES

Let us consider an incompressible, Newtonian fluid in a bounded domain $\Omega \subset \mathbb{R}^d$, $d = 2, 3$, modeled through the Navier-Stokes Equations in convective form for the velocity $\boldsymbol{u}(t) : \Omega \to \mathbb{R}^d$ and the pressure $p(t) : \Omega \to \mathbb{R}$:

$$\begin{cases} \rho \partial_t \boldsymbol{u} + \rho(\boldsymbol{u} \cdot \boldsymbol{\nabla})\boldsymbol{u} - \mu \Delta \boldsymbol{u} + \boldsymbol{\nabla} p = \boldsymbol{0} & \text{in} \quad \Omega, \\ \boldsymbol{\nabla} \cdot \boldsymbol{u} = 0 & \text{in} \quad \Omega \end{cases} \tag{1}$$

where ρ stands for the density and μ denotes the dynamic viscosity. Moreover, we consider homogeneous initial condition $\boldsymbol{u}(0, \boldsymbol{x}) = \boldsymbol{0}$, $\forall \boldsymbol{x} \in \Omega$. At this point, we observe that the methods for handling backflow at open boundaries can be defined independently of the chosen formulation of the viscous term (either using the strain rate tensor or the Laplacian). In the rest of the paper, we will focus on the Laplacian formulation. It is worth noticing that in the regimes of physiological interest that are treated in this work the viscous forces are small compared with the pressure forces. For the sake of completeness, it is worth mentioning that we have performed additional numerical tests using the strain rate tensor formulation, which yielded very similar outcome (results omitted).

In order to define the boundary conditions, we subdivide the boundary as $\partial\Omega = \Gamma_D \cup \Gamma_N$. Then, the Dirichlet boundary conditions are defined as

$$\boldsymbol{u} = \boldsymbol{u}_D \quad \text{on} \quad \Gamma_D \tag{2}$$

where $\boldsymbol{u}_D$ is a given velocity data, and the natural (or Neumann) boundary conditions are defined as

$$(\mu \boldsymbol{\nabla} \boldsymbol{u} - p\boldsymbol{1})\boldsymbol{n} = \boldsymbol{g}_N \quad \text{on} \quad \Gamma_N \tag{3}$$

DOI: 10.1002/cnm.2918

(where $\mathbf{1}$ denotes the d-dimensional identity matrix). The set Γ_N is usually denoted in the literature as *open boundary*.

As next, let us denote with $(\cdot,\cdot)_X$ the usual scalar product in the Hilbert space of Lebesgue integrable functions $L^2(X)$, for an open set $X \subset \mathbb{R}^d$, being $\|\cdot\|_{0,X}$ the associated norm. Furthermore, we use the standard notation $H^1(\Omega)$ for the Sobolev space with weak (first) derivatives in $L^2(\Omega)$ and define the space

$$H^1_0(\Omega) = \{\boldsymbol{v} \in H^1(\Omega) \mid \boldsymbol{v}_{|\Gamma_D} = 0\}.$$

Then, the weak formulation of Problem (1) reads: For all $0 < t \leq T$, find $\boldsymbol{u}(t) \in H^1(\Omega)$, satisfying the Dirichlet boundary condition (2), and $p(t) \in L^2(\Omega)$, such that

$$\begin{cases} \mathcal{A}(\boldsymbol{u},\boldsymbol{v}) - \mathcal{B}(p,\boldsymbol{v}) = (\mathbf{g}_N,\boldsymbol{v})_{\Gamma_N}\,, \\ \mathcal{B}(q,\boldsymbol{u}) = 0 \end{cases} \tag{4}$$

for all $\boldsymbol{v} \in H^1_0(\Omega)$ and $q \in L^2(\Omega)$, with the common definitions of the variational forms:

$$\begin{aligned} \mathcal{A}(\boldsymbol{u},\boldsymbol{v}) &:= \rho\,(\partial_t \boldsymbol{u},\boldsymbol{v})_\Omega + \rho\,((\boldsymbol{u}\cdot\boldsymbol{\nabla})\boldsymbol{u},\boldsymbol{v})_\Omega + \mu\,(\boldsymbol{\nabla}\boldsymbol{u},\boldsymbol{\nabla}\boldsymbol{v})_\Omega + \frac{\rho}{2}\,((\boldsymbol{\nabla}\cdot\boldsymbol{u})\boldsymbol{u},\boldsymbol{v})_\Omega\,, \\ \mathcal{B}(p,\boldsymbol{v}) &:= (p,\boldsymbol{\nabla}\cdot\boldsymbol{v})_\Omega\,, \end{aligned} \tag{5}$$

where the last integral in $\mathcal{A}(\boldsymbol{u},\boldsymbol{v})$ corresponds to the strongly consistent Temam stabilization [37], used for improving the energy balance at the space-semidiscrete level, since the divergence-free condition holds in general only in a weak sense. Note that using the conservative form of the advection term, the Temam term to be included has the same form, but with opposite sign.

Testing the formulation (4) with $(\boldsymbol{v},q) = (\boldsymbol{u},p)$ and using standard arguments, see, e.g., [20], one obtains the following energy balance in the non-forced case ($\boldsymbol{u}_D = \mathbf{g}_N = \mathbf{0}$)

$$\frac{\mathrm{d}}{\mathrm{d}t}E_\Omega(t) = -D_\Omega(t) - \frac{\rho}{2}\left(|\boldsymbol{u}|^2, \boldsymbol{u}\cdot\boldsymbol{n}\right)_{\Gamma_N}\,, \tag{6}$$

where

$$E_\Omega(t) := \frac{\rho}{2}\|\boldsymbol{u}\|^2_{0,\Omega}\,,\quad D_\Omega(t) := \mu\|\boldsymbol{\nabla}\boldsymbol{u}\|^2_{0,\Omega}$$

denote the kinetic energy and the viscous dissipation of the fluid, respectively.

In particular, in presence of backflow across a subset of Γ_N (i.e., when $\boldsymbol{u}\cdot\boldsymbol{n} < 0$), the last term in the right-hand-side of (6) leads to an incoming energy, and can in general not be compensated by the viscous dissipation term. Thus, a stable energy balance cannot be guaranteed. In practice, these instabilities might yield unphysical oscillations that affect the feasibility and reliability of the numerical simulations, already for moderate Reynolds numbers. Tackling this issue is crucial for the numerical simulation of physiological flows, such as blood flow in large arteries and air flow in the respiratory tract.

It is worth mentioning that the stability issues in presence of backflow pointed out in (6) do not depend on the particular formulation of the advection term in the Navier–Stokes equations: for both the convective form $(\mathbf{u}\cdot\nabla)\mathbf{u}$ and the conservative form $\nabla\cdot(\mathbf{u}\otimes\mathbf{u})$, if the Neumann boundary condition (3) is imposed, the same boundary term $\rho/2(|\mathbf{u}|^2,\mathbf{u}\cdot\mathbf{n})$ arises.

3. AN OVERVIEW OF BACKFLOW TREATMENTS

In what follows, we will consider the following stabilized version of the weak formulation (4): For all $0 < t \leq T$, find $\boldsymbol{u}(t) \in H^1(\Omega)$, satisfying the Dirichlet boundary conditions (2), and $p(t) \in L^2(\Omega)$, such that

$$\begin{cases} \mathcal{A}(\boldsymbol{u},\boldsymbol{v}) - \mathcal{B}(p,\boldsymbol{v}) + \mathcal{S}_{\Gamma_N}(\boldsymbol{u},\boldsymbol{v}) = (\mathbf{g}_N,\boldsymbol{v})_{\Gamma_N}\,, \\ \mathcal{B}(q,\boldsymbol{u}) = 0 \end{cases} \tag{7}$$

DOI: 10.1002/cnm.2918

for all $\boldsymbol{v} \in H_0^1(\Omega)$ and $q \in L^2(\Omega)$, where $\mathcal{S}_{\Gamma_N}(\boldsymbol{u}, \boldsymbol{v})$ denotes a stabilization term accounting for backflow instabilities across the boundary Γ_N. In particular, in the following parts of the section we will overview several forms of $\mathcal{S}_{\Gamma_N}(\boldsymbol{u}, \boldsymbol{v})$ that have been proposed in the literature. Moreover, a subsection will be dedicated also to a brief introduction to the so-called *method of characteristics*, which is based on the discretization of the total time derivative, without additional stabilization terms.

3.1. Velocity-penalization methods

The first class of stabilization terms, considered in this paper, is based on a modification of the Neumann boundary condition (3) as

$$(\mu \boldsymbol{\nabla} \boldsymbol{u} - p\mathbf{1})\boldsymbol{n} + \beta \frac{\rho}{2} \mathbf{f}(\boldsymbol{u}) = \mathbf{g}_N \quad \text{on } \Gamma_N \,, \tag{8}$$

where $\beta > 0$ is considered a free parameter. In the context of Galerkin methods, Equation (8) leads to stabilization terms of the form $\mathcal{S}_{\Gamma_N}(\boldsymbol{u}, \boldsymbol{v}) = \beta \frac{\rho}{2} (\mathbf{f}(\boldsymbol{u}), \boldsymbol{v})_{\Gamma_N}$. In what follows, the different forms reported for $\mathbf{f}(\boldsymbol{u})$ in the literature will be reviewed in a chronological order.

To the authors best knowledge, the first proposal appeared in [5], with the definition

$$\mathbf{f}(\boldsymbol{u}) = -|\boldsymbol{u}|^2 \boldsymbol{n} \,. \tag{9}$$

Note that this results in a stabilization term on Γ_N which is different from zero also in the case of pure outflow, i.e. for $\boldsymbol{u} \cdot \boldsymbol{n} \geq 0$ on entire Γ_N. In [24] was shown that this choice yields stable but unphysical solutions when the term $(\rho/2)|\boldsymbol{u}|^2 \boldsymbol{n}$ is comparable with $\mathbf{g}_N$. However, the total pressure approach has been conveniently applied for coupling fluid models of different dimensions in a stable way, see, e.g., [19]. Boundary conditions including the $|\boldsymbol{u}|^2$-term have been applied only during backflow in the context of other methods [16, 17, 34]. More details will be provided at the end of this section (see, e.g., Equation (13)). However, it is worth noticing that, in order to guarantee overall energy stability, this term shall be discretized fully implicitly in time (for example, if combined with semi-implicit discretization of the convective term).

Subsequently, a whole family of boundary conditions in the form (8) was introduced in [14, 15], defining

$$\begin{aligned} \mathbf{f}(\boldsymbol{u}) = &\left(\alpha_0 |(\boldsymbol{u} - (1-2\alpha_1)\boldsymbol{u}_0) \cdot \boldsymbol{n}|^+ - (\boldsymbol{u} - (1-2\alpha_1)\boldsymbol{u}_0) \cdot \boldsymbol{n}\right)(\boldsymbol{u} - \boldsymbol{u}_0) + \dots \\ &\left(\alpha_0 |((1-\alpha_2)\boldsymbol{u} - (\alpha_2 - \alpha_3)\boldsymbol{u}_0) \cdot \boldsymbol{n}|^+ - ((1-\alpha_2)\boldsymbol{u} - (\alpha_2 - \alpha_3)\boldsymbol{u}_0) \cdot \boldsymbol{n}\right) \boldsymbol{u}_0 \end{aligned} \tag{10}$$

for a given velocity profile $\boldsymbol{u}_0 : \Gamma_N \to \mathbb{R}^2$ and given parameters $\alpha_0 \geq 0, \alpha_1, \alpha_2, \alpha_3 \in \mathbb{R}$, and where $|\cdot|^+$ denotes the positive part. Existence and uniqueness of weak solutions of the stabilized Navier-Stokes problem were proven for $\beta \geq 1.0$. Moreover, in this original version, it was proposed to choose $\boldsymbol{u}_0$ as the solution of a stationary Stokes flow satisfying the same boundary conditions.

In the remaining part of this study, we will not include this approach within the benchmarked methods, due to the difficulty, in practice, of choosing $\alpha_0, \alpha_1, \alpha_2, \alpha_3$. For the sake of completeness, it must be also mentioned that in the original publications [14, 15], the numerical analysis was based on a symmetric formulation for the stress tensor.

The choices $\alpha_0 = 1$, $\alpha_1 = 1/2$, $\alpha_2 = \alpha_3 = 1$ in Equation (10) lead to the modified boundary condition

$$\mathbf{f}(\boldsymbol{u}) = |\boldsymbol{u} \cdot \boldsymbol{n}|^- (\boldsymbol{u} - \boldsymbol{u}_0) \,, \tag{11}$$

where $|\boldsymbol{u} \cdot \boldsymbol{n}|^-$ denotes the negative part of the normal velocity. Hence, (11) results in a stabilization term active only during backflow. In the last years, different variants of (11) have been proposed in the literature in the context of physiological flows, all of them independently from the original work [14]. In particular, the choice $\boldsymbol{u}_0 = \mathbf{0}$ has been widely employed in both hemodynamics [2, 4, 18, 33] and respiratory regimes [29, 30]. While $\beta \geq 1$ assures energy

DOI: 10.1002/cnm.2918

stability, the numerical results of [18] showed that decreasing the value of the parameter up to $\beta = 0.4$ still yields stable solutions in the case of blood flow, thus suggesting that the lack of stability (and hence the magnitude of the required stabilization) depends on the considered flow regime.

For the boundary condition in the form (11), the existence of weak solutions was shown for $\boldsymbol{u}_0 = \mathbf{0}$ and $\beta \geq 1$ in combination with the non-symmetric formulation for the stress tensor in [13] and investigated for non-homogeneous fluids in [11]. A uniqueness result in the case of small data for $\beta \geq 1$ can be found in [12]. It is worth mentioning that, for sufficiently small data, the analysis of [3] stated the existence of regular solution of (1) in presence of open boundaries and without stabilization. These results confirms, to some extent, the observation of [18] on the possibility of decreasing the stabilization parameter β under certain flow conditions.

A further variant was proposed in [33], where $\boldsymbol{u}_0$ was taken as a plug profile for a given flow rate at the inlet of the ascending aorta.

A slightly different Neumann boundary condition was recently proposed in [22, 26], using

$$\mathbf{f}(\boldsymbol{u}) = \begin{cases} 0 & \text{for } \boldsymbol{u}\cdot\boldsymbol{n} \geq 0, \\ |\boldsymbol{u}\cdot\boldsymbol{n}|^{-}\boldsymbol{u} - |\boldsymbol{u}_0\cdot\boldsymbol{n}|^{-}\boldsymbol{u}_0 & \text{for } \boldsymbol{u}\cdot\boldsymbol{n} < 0, \end{cases} \tag{12}$$

and $\beta = 2.0$ which combines the features of both aforementioned schemes: it is only active during backflow (as in (11)) and both $\boldsymbol{u}$ and $\boldsymbol{u}_0$ terms are uncoupled (as in (9)). In particular, in [22] $\boldsymbol{u}_0$ was chosen as a parabolic profile whose magnitude was modulated by a given flow rate, in the context of respiratory mechanics. Then in [26], $\boldsymbol{u}_0$ was computed dynamically as a superposition of Womersley modes in order to obtain for $\boldsymbol{u}_0$ a more suitable approximation of the flow in the transient case, showing numerical examples for both blood and respiratory flows. In this case, the profile $\boldsymbol{u}_0$ might result complicated to implement in general situations, in particular on a boundary of arbitrary shape where no analytical solution is available. Therefore, in the numerical studies here we will consider a generalization of this approach by defining $\boldsymbol{u}_0$ as the solution to a Stokes problem on the same domain Ω and with the same boundary conditions than the Navier-Stokes problem of interest, as it was proposed in [14, 15] for the stabilization term in Equation (10). Notice that, in the case of a Womersley flow, this is equivalent to the method of [26].

A further approach which fits in the framework of velocity penalization method is the *convective-like* stabilization recently introduced in [34]. In this case, an inertia term is included in the Neumann boundary condition, which is defined by

$$\mu D_0 \frac{\partial \boldsymbol{u}}{\partial t} + (\mu \boldsymbol{\nabla}\boldsymbol{u} - p\mathbf{1})\boldsymbol{n} - \beta\frac{\rho}{2}\mathbf{f}(\boldsymbol{u}) = \mathbf{g}_N \quad \text{on } \Gamma_N\,, \tag{13}$$

with

$$\mathbf{f}(\boldsymbol{u}) = -\Theta_\delta\left(\boldsymbol{u}\cdot\boldsymbol{n}\right)\left(|\boldsymbol{u}|^2\boldsymbol{n} + (\boldsymbol{u}\cdot\boldsymbol{n})\boldsymbol{u}\right). \tag{14}$$

In (14), $\Theta_\delta(x) = 0.5(1 - \tanh(x/\delta))$, for $\delta \geq 0$ is a smooth approximation of a $|\operatorname{sgn}(x)|^-$ (taking value 1 for negative x, and value 0 otherwise), and D_0 is a free parameter. In particular, in [34] it is suggested to define $D_0 = \mathcal{O}\left(\frac{1}{U_c}\right)$, where U_c stands for the magnitude of the convective velocity, taking also $\beta = 1$. For the sake of completeness, we also mention the case $D_0 = 0$ had been previously proposed in [16, 17]. Moreover, notice also that, for small δ, (13) reduces to a linear combination of (11) and (9) (setting $\boldsymbol{u}_0 = 0$), what would ensure energy stability if $\beta = \frac{1}{2}$. However, in [34] $\beta = 1$ was used. For the sake of completeness, both the choices $\beta = \frac{1}{2}$ and $\beta = 1$ will be considered for the numerical tests.

Remark 1. *In [34] it was observed that the parameter D_0 has only very little influence on the numerical results. This behavior was confirmed by our numerical experiments (results mostly omitted). Therefore, in the sections dedicated to the numerical studies (Sections 4 and 5) we will only report the results concerning the case $D_0 = 0$.*

DOI: 10.1002/cnm.2918

3.2. Velocity gradient penalization methods

An alternative strategy, based on the penalization of the tangential derivatives of the velocity at the open boundary, was recently proposed in [6]. In contrast to the previous mentioned boundary conditions, the tangential derivative regularization can only be formulated in a variational form, e.g. in the form (7). Denoting the test function for the momentum Equation by $\boldsymbol{v}$ the corresponding additional semi-linear form reads

$$\mathcal{S}_{\Gamma_N}(\boldsymbol{u},\boldsymbol{v}) = \frac{\rho}{2}\gamma \sum_{j=1}^{d-1} \left(|\boldsymbol{u}\cdot\boldsymbol{n}|^{-}\boldsymbol{t}_j^{\intercal}\boldsymbol{\nabla}\boldsymbol{u}, \boldsymbol{t}_j^{\intercal}\boldsymbol{\nabla}\boldsymbol{v}\right)_{\Gamma_N}, \tag{15}$$

where γ is a stabilization parameter to be chosen, and the vectors $\boldsymbol{t}_1, \boldsymbol{t}_{d-1}$ stand for the tangential directions to Γ_N. The stabilization term does not require any assumption on the boundary velocity profile. Concerning the choice of the stabilization parameter, it was shown in [6] that energy stability can be ensured if γ is larger than the squared Poincaré constant of the domain Γ_N. However, in [6] it was suggested that the backflow instabilities of the highest frequencies of the discrete solution can be stabilized by choosing $\gamma = h^2/3$, where h denotes the mesh characteristic size. This implies in practice that in all reported numerical results the stabilization parameter can be reduced with the element mesh size while the whole solution remains stable.

In view of these considerations, in the numerical tests considered in this paper the stabilization parameter will be defined as

$$\gamma = \gamma_0 \frac{h^2}{3},$$

considering then different choices of γ_0.

Finally, an extension of (15) proposed in [7] is based on the stabilization term

$$\mathcal{S}_{\Gamma_N}(\boldsymbol{u},\boldsymbol{v}) = l_e \int_{\Gamma_N} (\rho\partial_t\boldsymbol{u} + a(t)\boldsymbol{n})\cdot\boldsymbol{v} + \mu\mathcal{V}(\boldsymbol{u},\boldsymbol{v}), \tag{16}$$

with

$$\begin{aligned} \mathcal{V}(\boldsymbol{u},\boldsymbol{v}) &:= \sum_{j=1}^{d-1} \psi(\boldsymbol{t}_j,\boldsymbol{n};\boldsymbol{u},\boldsymbol{v}) + \sum_{i,j=1}^{d-1} \psi(\boldsymbol{t}_j,\boldsymbol{t}_i;\boldsymbol{u},\boldsymbol{v}) \\ \psi(\boldsymbol{s}_1,\boldsymbol{s}_2;\boldsymbol{u},\boldsymbol{v}) &:= (\boldsymbol{s}_1^{\intercal}\boldsymbol{\nabla}(\boldsymbol{v}\cdot\boldsymbol{s}_2))^{\intercal}\,(\boldsymbol{s}_1^{\intercal}\boldsymbol{\nabla}(\boldsymbol{u}\cdot\boldsymbol{s}_2)) \end{aligned} \tag{17}$$

where l_e can be related to the problem parameters via

$$l_e = \frac{\rho U_b \sigma}{2\mu}, \tag{18}$$

U_b being the peak backflow velocity on the open boundary at the previous time step and σ standing for a free stabilization parameter [7]. The function $a(t)$ in (16) plays the role of an approximated boundary pressure gradient that can be computed explicitly during the simulation by mean of the simple lumped parameter model

$$a(t) = -L\dot{Q}(t) - rQ(t),$$

where $Q(t)$ denotes the flow rate, $L = \rho/|\Gamma_N|$ and r is an approximate resistance updated as detailed in [7, Equation (16)]. The resulting formulation at the outlet is weakly consistent with a Stokes flow along the normal direction driven by a pressure gradient $a(t)$. As in the case of the tangential regularization, numerical results showed that the parameter σ can be reduced with the mesh size [7]. As suggested in [7] for the numerical study considered in this paper the

DOI: 10.1002/cnm.2918

stabilization parameter will be defined as

$$\sigma = \sigma_0 \frac{h^2}{3},$$

where h denotes the mesh characteristic size.

In what follows, we will refer to (16) as the Stokes-residual stabilization.

3.3. Method of characteristics

The method of characteristics, introduced in [32] and also known as Characteristic - Galerkin [31], has been recently tested for the numerical treatment of open boundaries in presence of backflow [20]. The satisfactory results reported by [20] motivate a more detailed study, and therefore this approach will be taken into account in the context of this benchmark study.

The method is based on the idea of treating the convection term within a time discretization of a total derivative along the *characteristic* curves, i.e.,

$$\partial_t \boldsymbol{u}(\gamma(t),t) + \boldsymbol{u}(\gamma(t),t)\cdot\nabla\boldsymbol{u}(\gamma(t),t) = \frac{d}{dt}\boldsymbol{u}(\gamma(t),t)\,, \tag{19}$$

where the curve $\gamma(t)$ satisfies $\dot{\gamma}(t) = \boldsymbol{u}(\gamma(t),t)$.

In order to briefly introduce the method, let n denote a given time step, and let us consider the ordinary differential equation describing a characteristic curve in the time interval $[t^n, t^{n+1}]$ passing through $\boldsymbol{x}$ at time t^{n+1}:

$$\begin{aligned} &\frac{dX^n_{\boldsymbol{x}}}{d\tau}(\tau) = \boldsymbol{u}(X^n_{\boldsymbol{x}}(\tau),\tau),\ \tau\in[t^n,t^{n+1}] \\ &X^n_{\boldsymbol{x}}(t^{n+1}) = \boldsymbol{x}\,. \end{aligned} \tag{20}$$

In particular, the point $X^n_{\boldsymbol{x}}(t^n)$ is denoted as the foot of the characteristic.

Hence, for a given $\boldsymbol{x}\in\Omega$, using the above definition of $X^n_{\boldsymbol{x}}(\tau)$ equation (19) can be discretized using a first-order approximation as

$$\begin{aligned} \partial_t \boldsymbol{u}(\boldsymbol{x},t^{n+1}) + \boldsymbol{u}(\boldsymbol{x},t^{n+1})\cdot\nabla\boldsymbol{u}(\boldsymbol{x},t^{n+1}) &= \frac{d}{dt}\boldsymbol{u}(\boldsymbol{x},t^{n+1}) \\ &\approx \frac{1}{\delta t}\left(\boldsymbol{u}(\underbrace{X^n_{\boldsymbol{x}}(t^{n+1})}_{\boldsymbol{x}},t^{n+1}) - \boldsymbol{u}(X^n_{\boldsymbol{x}}(t^n),t^n)\right) \end{aligned} \tag{21}$$

(see, e.g, [10] for schemes based on a higher-order time discretization).

Notice that, in general, (20) might not be well defined if, for some $\tau\in[t^n,t^{n+1}]$, $X^n_{\boldsymbol{x}}(\tau)$ lies outside of Ω. In particular, this is the case of backflow boundaries, where $\boldsymbol{u}(\boldsymbol{x})\cdot\boldsymbol{n}<0$, for some $\boldsymbol{x}\in\partial\Omega$. In order to overcome this issue, the approximation (21) is modified replacing the foot of the characteristic $X^n_{\boldsymbol{x}}(t^n)$ with the point where the considered characteristic intersects the boundary. To do this, one can define the operator[†]

$$\hat{X}^n(\boldsymbol{x}) = X^n_{\boldsymbol{x}}(\tau^*_n),\ \text{with}\ \tau^*_n = \min\left\{\tau\in[t^n,t^{n+1}] | X^n_{\boldsymbol{x}}(\tau)\in\Omega\right\}\,. \tag{22}$$

Notice that, by construction, $\hat{X}^n(\boldsymbol{x})\in\Omega$, for all $\boldsymbol{x}\in\Omega$. Then, the term $X^n_{\boldsymbol{x}}(t^n)$ in (21) is replaced by $\hat{X}^n(\boldsymbol{x})$.

The characteristic method for the Navier–Stokes Equations can be formulated as the solution of the following time-semidiscrete problem at each time step t^{n+1}: Find $\boldsymbol{u}^{n+1}\in H^1(\Omega)$,

[†]In Freefem++ the computation of the foot of the characteristics is implemented for two-dimensional and for three-dimensional problems via the operator `convect` (the C++ code is freely available).

satisfying the Dirichlet boundary conditions (2), and $p^{n+1} \in L^2(\Omega)$, such that

$$\begin{aligned} &\frac{\rho}{\delta t}\left(\boldsymbol{u}^{n+1}, \boldsymbol{v}\right)_\Omega + \mu\left(\nabla \boldsymbol{u}^{n+1}, \nabla \boldsymbol{v}\right)_\Omega - \left(p^{n+1}, \nabla \cdot \boldsymbol{v}\right)_\Omega - \left(q, \nabla \cdot \boldsymbol{u}^{n+1}\right)_\Omega \\ &= \frac{\rho}{\delta t}\left(\boldsymbol{u}^n \circ \hat{X}^n, \boldsymbol{v}\right)_\Omega + (\mathbf{g}_N, \boldsymbol{v})_{\Gamma_N} \end{aligned} \tag{23}$$

for all $\boldsymbol{v} \in H^1(\Omega)$, zero on Γ_D and all $q \in L^2(\Omega)$.

The main advantage of the method of characteristics is that the Navier–Stokes Equations are reduced to a linear (Stokes) system, for which the finite element matrix can be assembled only once. However, the price to pay is that the method requires, at each step, multiple integrations of the characteristic (20) (e.g., at each Gauss point required for numerical integration). This step might be computationally expensive, depending also on the properties of the velocity field that may require a high order time integration or a smaller time step.

To the best of our knowledge, there are no results ensuring general stability for this method. In particular, in the energy-based stability analysis reported in [36] showed that for the method of characteristics it holds an energy balance analogous to (6), including the destabilizing backflow term, up to higher order terms in δt. However, whether these additional terms may have a stabilizing effects is still unclear.

3.4. Other strategies for backflow treatment not considered in this study

For the sake of completeness, it has to be mentioned that other approaches to avoid backflow instabilities have been proposed, based on constraints of the velocity profile on the open boundary. In particular, a first method [27] imposes a given velocity profile (dynamically scaled by the flow rate) through Lagrange multipliers. However, its implementation might result particularly intrusive, and, at the same time, it shifts the local velocity instability issues to the global equilibria of fluxes.

A second approach enforces the velocity to be normal to the boundary (see, e.g., [8, 18]) and it is often used in simulation practice, as it can be implemented adding simply a penalization term at the weak level. However, in view of (6), it does not guarantee energy stability, as it does not remove the issue of the uncontrolled incoming energy due to the (normal) incoming velocity. Nevertheless, in practice (i.e., at the discrete level), enforcing zero tangential velocity might reduce, or delay, the arise of instabilities, and hence be effective for low backflow regimes. It was shown in [18] that these two approaches may not deliver satisfactory results in terms of stability and accuracy in hemodynamics relevant regimes.

A further method, recently proposed in [2], consists in plugging a 3D extension to the boundary where the Navier-Stokes Equations are modified with resistive and compressibility terms to obtain an equivalent energy balance to a standard coupling with a 3-element Windkessel model, and therefore it is suited for biofluid multiscale simulations. However, the imposition of general Neumann boundary conditions is not straightforward, and therefore this method was not considered here.

The interested reader is also referred to [20] for a recent review of algorithmic and theoretical aspects of the treatment of boundary conditions and backflow, where the velocity penalization stabilizations and the total pressure formulations are discussed, as well as the treatment of the advection and viscous terms.

3.5. Summary of considered methods

When presenting the numerical results, the methods overviewed above will be denoted as follows:

1. VEL($\boldsymbol{u}_0, \beta$): Stabilization term obtained using the boundary condition (8) for a given β and with $\mathbf{f}(\mathbf{u})$ in the form of (12). We will consider the correcting velocity $\boldsymbol{u}_0 = \mathbf{0}$ and $\boldsymbol{u}_0 = \boldsymbol{u}_S$ (the solution to a Stokes problem with the same Dirichlet and Neumann boundary conditions of the target Navier-Stokes problem), together with different values

DOI: 10.1002/cnm.2918

of the parameter β. In particular, we will test the method with β=0.1, 0.2, 0.5, 1.0 (that guarantees unconditional stability), 2.0 (used in [22]);
2. Vel-Press (β): Stabilization (13) for a given β with parameter $D_0 = 0$ (see Remark 1). In the numerical tests, $\beta = 1.0$ and $\beta = 0.5$ will be considered;
3. Tangential Reg(γ_0): Stabilization term (15) [6]. We will consider the values $\gamma_0 = 0.1$, 0.2, 0.5, 1.0 (recommended in [6]), 2.0; moreover, with Tangential Reg(P) we will denote the method defined taking γ equal to the squared Poincaré constant of the open boundary (that assures unconditional stability);
4. Stokes-Residual(σ_0): Stabilization term (16) [7]. As for the tangential regularization, we will consider the values $\sigma_0 =$ 0.1, 0.2, 0.5, 1.0, 2.0; moreover, with Stokes-Residual(P) we will denote the method defined taking σ equal to the squared Poincaré constant of the open boundary (that assures unconditional stability);
5. Characteristics: methods of characteristics of first order (i.e., Problem (23)).

4. BENCHMARK 1: REVERSED FLOW IN A STRAIGHT CHANNEL

The first example consists of a time-dependent reverse flow in a channel with an asymmetric inflow. The goal of this test case is to assess the performance of the backflow stabilization treatments in situations of large backflow, without necessarily the presence of vortices, as it can be encountered in the blood flows and airway portions branching from the main vessel.

It is worth noticing that the so-called Womersley flow (a channel flow with an oscillating unidirectional pressure drop), for which an analytical solution is available, is close to this setting. However, due to symmetry reasons, the convection term for a Womersley flow vanishes, so that the Navier-Stokes and the (linear) Stokes Equation admits the same solution. For this reason, this test is not suited for a benchmark study, as the stabilization methods based on Stokes solutions (Vel($\boldsymbol{u}_S, \beta$) and Stokes-Res(σ_0)), by construction, would deliver better results. However, it is worth noticing that a benchmark based on a Womersley flow may be useful for validating the implementation of the different backflow stabilization methods, since, depending on the discretization, spurious convection effects appear, which might yield to backflow instabilities. For the interested reader, we refer to [6, 7, 22, 26] for numerical examples considering Womersley flows.

4.1. Benchmark setting

We construct a channel flow using an inflow boundary condition obtained asymmetrizing a Womersley solution. In particular, We consider a two-dimensional square $\Omega = [0, L]^2$ with $\Gamma_{\text{in}} = \{(x, y) \in \Omega \mid y = 0\}$, $\Gamma_0 = \{(x, y) \in \Omega \mid x = \{0, L\}\}$ and $\Gamma_{\text{out}} = \{(x, y) \in \Omega \mid y = L\}$, with $L =$ 1 cm. In the hemodynamic regime, the diameter (1cm) corresponds to the one of the secondary branches (e.g. supra-aortic, renal arteries, etc), where backflow typically occurs in blood flow applications. In respiratory flows this diameter corresponds to the main bronchi (generation 1 or 2).

As next, we consider a Womersley profile

$$W(x,t) \quad = \quad \sum_{k=0}^{K} d_k \Psi_k(t) S_k(x) \tag{24}$$

DOI: 10.1002/cnm.2918

with $K = 19$ and

$$\begin{aligned} d_k &= \frac{4\Delta P}{\rho\pi(2k+1)((2k+1)^4\sigma^2\pi^4+\omega^2)}, \\ \sigma &= \frac{\mu}{\rho L^2}, \\ S_k(x) &= \sin\left(\pi(2k+1)\frac{x}{L}\right), \\ \Psi_k(t) &= (2k+1)^2\sigma\pi^2\sin(\omega t) - \omega\cos(\omega t) + \omega\exp^{-(2k+1)^2\sigma\pi^2 t}. \end{aligned}$$

The profile (24) depends on the peak pressure drop per length ΔP, the frequency ω, the density ρ and the viscosity μ. These physical parameters are chosen in order to represent typical blood or air regimes, see Sections 4.4 and 4.5 for more details.

Then, in order to break the symmetry of the Womersley flow, and hence to obtain non-vanishing convective effects, we define a *reference* problem on Ω imposing on Γ_{in} the asymmetric Dirichlet data

$$\boldsymbol{u}_{\text{D}} = (0, v(x,t)),\ v(x,t) = \frac{3}{2}x^{0.7}W(x,t). \tag{25}$$

We consider then the Navier-Stokes Problem (1) with boundary conditions

$$\begin{cases} \boldsymbol{u}_{\text{ref}} = \boldsymbol{u}_{\text{D}} & \text{on} \quad \Gamma_{\text{in}}, \\ \boldsymbol{u}_{\text{ref}} = \boldsymbol{0} & \text{on} \quad \Gamma_0, \\ (\mu\boldsymbol{\nabla}\boldsymbol{u}_{\text{ref}} - p_{\text{ref}}\boldsymbol{1})\boldsymbol{n} = \boldsymbol{0} & \text{on} \quad \Gamma_{\text{out}}. \end{cases} \tag{26}$$

which can be solved without the need of backflow stabilization, since at the inflow boundary a Dirichlet boundary condition is imposed, while on the open boundary no reverse flow appear in the simulated time window. In what follows, we will denote the corresponding solution $(\boldsymbol{u}_{\text{ref}}, p_{\text{ref}})$ as the *reference solution*.

As next, let $(\boldsymbol{u}_{\text{back}}, p_{\text{back}})$ be the solution of a second problem, obtained imposing a no-slip boundary condition on Γ_0, a homogeneous Neumann boundary condition on Γ_{out}, and a Neumann boundary condition consistent with the reference solution on Γ_{in}, i.e.

$$\begin{cases} (\mu\boldsymbol{\nabla}\boldsymbol{u}_{\text{back}} - p_{\text{back}}\boldsymbol{1})\boldsymbol{n} = (\mu\boldsymbol{\nabla}\boldsymbol{u}_{\text{ref}} - p_{\text{ref}}\boldsymbol{1})\boldsymbol{n} & \text{on} \quad \Gamma_{\text{in}}, \\ \boldsymbol{u}_{\text{back}} = \boldsymbol{0} & \text{on} \quad \Gamma_0, \\ (\mu\boldsymbol{\nabla}\boldsymbol{u}_{\text{back}} - p_{\text{back}}\boldsymbol{1})\boldsymbol{n} = \boldsymbol{0} & \text{on} \quad \Gamma_{\text{out}}, \end{cases} \tag{27}$$

Due to the application of the Neumann condition $(27)_1$ on the inflow boundary, the solution $(\boldsymbol{u}_{\text{back}}, p_{\text{back}})$ becomes quickly unstable in the numerical simulations, hence requiring an *ad hoc* treatment of the open boundary. Hence, in order to investigate the performances of stabilization methods, we monitor the differences between the numerical solutions $(\boldsymbol{u}_{\text{ref}}, p_{\text{ref}})$ (without stabilization) and $(\boldsymbol{u}_{\text{back}}, p_{\text{back}})$ (with backflow stabilization).

This benchmark consists then of the following two steps:

- Solve the reference problem: Find $\boldsymbol{u}_{\text{ref}}(t) \in H^1(\Omega)$, satisfying the Dirichlet boundary conditions $(26)_{1-2}$, $p_{\text{ref}}(t) \in L^2(\Omega)$, for all $0 < t \leq T$, such that

$$\begin{cases} \mathcal{A}(\boldsymbol{u}_{\text{ref}}, \boldsymbol{v}) - \mathcal{B}(p_{\text{ref}}, \boldsymbol{v}) = 0\,, \\ \mathcal{B}(q, \boldsymbol{u}_{\text{ref}}) = 0 \end{cases} \tag{28}$$

  for all $\boldsymbol{v} \in H^1_0(\Omega)$ and $q \in L^2(\Omega)$.
- Solve the stabilized problem: Find $\boldsymbol{u}_{\text{back}}(t) \in H^1(\Omega)$, satisfying the Dirichlet boundary condition $(27)_2$, $p_{\text{back}}(t) \in L^2(\Omega)$, for all $0 < t \leq T$, such that

$$\begin{cases} \mathcal{A}(\boldsymbol{u}_{\text{back}}, \boldsymbol{v}) - \mathcal{B}(p_{\text{back}}, \boldsymbol{v}) + \mathcal{S}_{\Gamma_{\text{in}}}(\boldsymbol{u}_{\text{back}}, \boldsymbol{v}) = (\mu\partial_{\boldsymbol{n}}\boldsymbol{u}_{\text{ref}} - p_{\text{ref}}\boldsymbol{n}, \boldsymbol{v})_{\Gamma_{\text{in}}}\,, \\ \mathcal{B}(q, \boldsymbol{u}_{\text{back}}) = 0 \end{cases} \tag{29}$$

DOI: 10.1002/cnm.2918

for all $\boldsymbol{v} \in H_0^1(\Omega)$ and $q \in L^2(\Omega)$. Note that the stabilization methods detailed in Section 3.5 are applied only on Γ_{in}.

It is worth mentioning that the locally resolved Neumann load used in (29) is required in order to test the accuracy of the different methods against a true reference solution and to avoid introducing additional errors due to, e.g., load averaging.

Within this study, we will also investigate the effect of imposing an additional constraint on the boundary, i.e., setting the tangential velocity to zero. This condition, which is consistent with the solution in this particular case, is generally known to improve the stability of the numerical simulations [18], as well as to enhance the regularity of the solution at the continuum level.

4.2. Space-time discretization

The numerical solutions to the different problems have been computed using a monolithic (saddle-point) formulation of the Navier-Stokes Equations. For the discretization in space, inf-sup stable Taylor-Hood $\mathbb{P}_2/\mathbb{P}_1$ finite elements have been used. This choice avoids the need of an additional stabilization, which would yield numerical results dependent on the choice of the stabilizing term. The time derivative of the velocity is semi-discretized with a backward Euler method, but the advective velocity in the convection term is treated explicitly and hence non-linear iterations are not needed. This allows also to treat the backflow velocity explicitly in the backflow stabilization methods. Moreover, for the particular choice of spatial and temporal discretization, an additional stabilization for the convection (e.g., SUPG) was not needed, since the numerical simulations in the reference problem remain stable in the time range of interest.

As already mentioned above, the benchmark problem can be defined independently of the discretization (i.e., mesh, finite element spaces or time step) and of the numerical approximation of the boundary data (discretization of the inflow profile for the Dirichlet boundary and approximation of the load vector on the open boundary).

4.3. Practical aspects of the benchmark setup

The numerical results have been computed following the steps detailed below. All the data needed to compute the numerical results shown in the following sections (meshes, boundary data, and simulation code) are available online[‡].

Discretization. An unstructured triangular mesh of the unit square has been generated, specifying the mesh characteristic size h. The mesh has been created using FreeFem++.

Solution of reference problem Problem (28) has been solved with the specified inflow Dirichlet boundary conditions (using FreeFem++).

Computation of boundary data With the chosen finite element spaces, the vector

$$\mathbf{T}_{\text{ref}} = (\mu \partial_{\boldsymbol{n}} \boldsymbol{u}_{\text{ref}} - p_{\text{ref}} \boldsymbol{n})$$

(with $\boldsymbol{n} = (0, -1)$) has been computed, which has to be imposed as natural boundary condition on Γ_{in}. in Problem (29).

Notice that, using $\mathbb{P}_2/\mathbb{P}_1$ finite elements, $\mathbf{T}_{\text{ref}}$ belongs to the space $\mathbb{P}_1^d$ of piecewise discontinuous functions. However, in order to make the benchmark independent of the choice of finite element spaces and to favor the reproducibility by different solvers (i.e., also by the solvers that require nodal values of input boundary data), the load in Problem (29) has been defined considering the L_2-projection of $\mathbf{T}_{\text{ref}}$ onto the space of piecewise continuous linear function.

[‡]See http://wias-berlin.de/people/caiazzo/backflow/

DOI: 10.1002/cnm.2918

Namely, we solved the linear systems defined by

$$\begin{aligned} &\int_\Omega \hat{T}_x v - \mu \partial_y u_{\mathrm{ref},x} v = 0, \quad \forall v \in \mathbb{P}_1 \\ &\int_\Omega \hat{T}_y v - (\mu \partial_y u_{\mathrm{ref},y} - p_{\mathrm{ref}} n_y) v = 0, \quad \forall v \in \mathbb{P}_1 \end{aligned} \tag{30}$$

imposing then the load $\hat{\mathbf{T}} = (\hat{T}_x, \hat{T}_y)$ on Γ_{in}.

Solution of backflow problem With the vector $\hat{\mathbf{T}}$, available at all boundary nodes, Problem (29) has been solved (using FreeFem++).

Evaluation The difference between the numerical solutions has been evaluated in terms of incoming flow $Q_{\mathrm{in}}(\boldsymbol{u}) = \int_{\Gamma_{\mathrm{in}}} \boldsymbol{u} \cdot \boldsymbol{n}$, average pressure drop

$$\Delta(p) = \frac{1}{|\Gamma_{\mathrm{in}}|} \int_{\Gamma_{\mathrm{in}}} p - \frac{1}{|\Gamma_{\mathrm{out}}|} \int_{\Gamma_{\mathrm{out}}} p$$

and monitoring the difference between the velocity and pressure profiles on the boundary Γ_{in}.

4.4. Numerical results for hemodynamics regime

The first set of numerical tests is carried out considering a hemodynamics regime, i.e.,

$$\rho = 1.06\,\mathrm{g/cm}^3,\ \mu = 0.035\,\mathrm{Poise},\ \Delta P = 400\,\mathrm{bary/cm}\ (\approx 0.3\,\mathrm{mmHg/cm}),\ \omega = 2\pi\,\mathrm{rad/s},$$

where the choice of ω is dictated by the order of magnitude of the length of a cardiac cycle (about 1 second). The peak Reynolds number amounts to 4400.

Figure 2 shows the corresponding reference solutions for velocity and pressure at peak backflow instant ($t = 0.48$ s), using a mesh characteristic size $h = 0.02$ cm and a time step $\delta t = 0.005$ s.

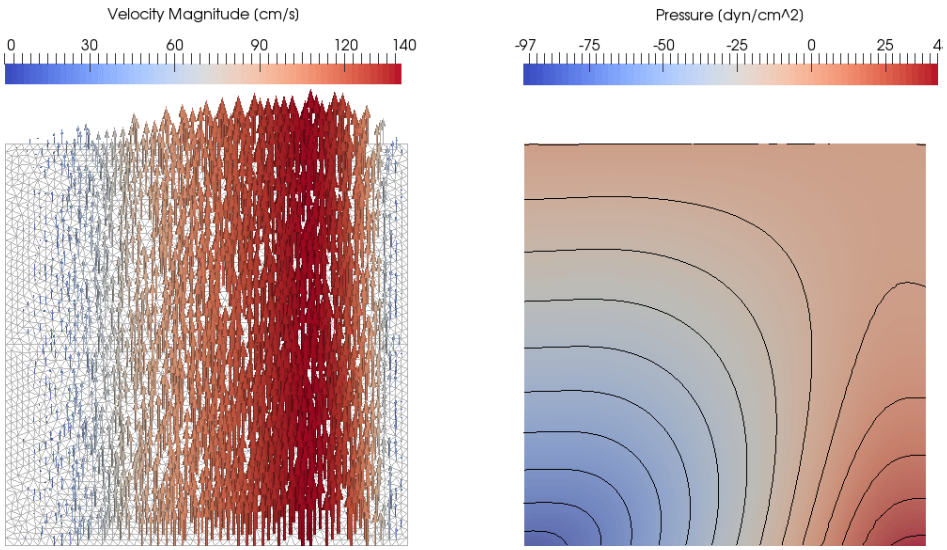

Figure 2. Reference solution (Benchmark 1, blood regime) at peak backflow (t=0.48s). Left: Mesh and glyph vector plot of the velocity field. Right: Pressure isolines.

We consider the time interval [0,0.5 s]. Without any stabilization, oscillations appear around time t=0.2 s, eventually leading to solution blow up. A preliminary verification step, in order

DOI: 10.1002/cnm.2918

to demonstrate that the arise of instability is due exclusively to the presence of backflow, was defined employing backflow stabilization consistent with the reference solution, and comparing the result with the reference solution itself. For this, we solve the backflow problem using the boundary condition modified as in (11), with $\boldsymbol{u}_0 = \boldsymbol{u}_{\text{ref}}$. The results shown in Figure 3 confirm that using a backflow stabilization consistent with the reference solution yields accurate results.

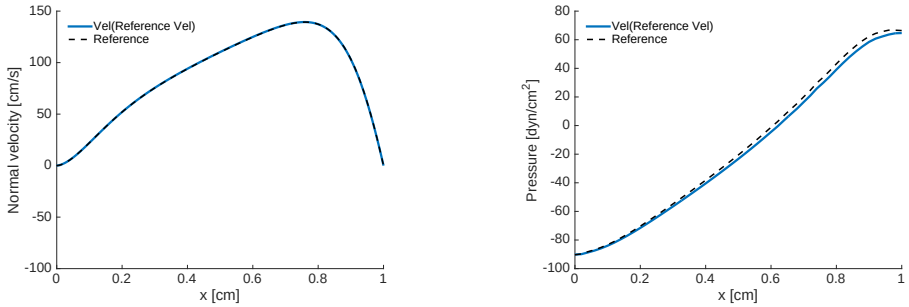

Figure 3. Benchmark 1, blood regime: Profiles of velocity (left) and pressure (right) at the inflow boundary (peak backflow, $t = 0.48$ s), using an open boundary stabilization based on a velocity penalization towards the reference velocity.

Figures 4-5 and Figures 6-7 show the incoming flow rate and the average pressure drop, respectively, considering the methods and parameter choices from Section 3.5. In particular, Figures 5 and 7 refer to the results including the additional constraint on vanishing tangential velocity to zero on the open boundary.

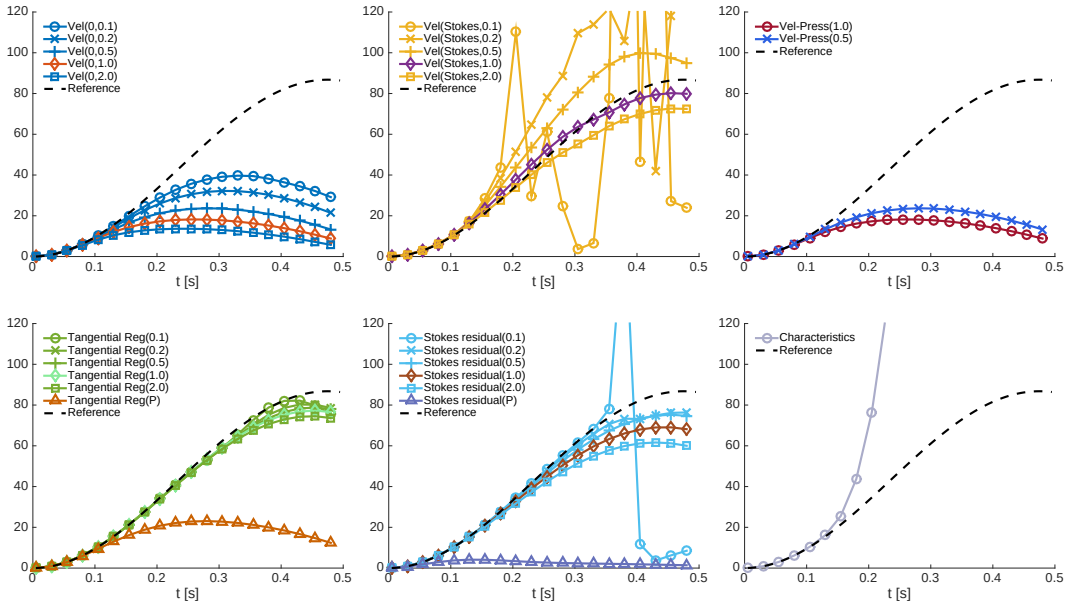

Figure 4. Benchmark 1 (full backflow), blood regime: incoming flow rate [cm^2/s] over time [s].

Several important aspects concerning the performance of the different methods can be appreciated from these pictures. Firstly, penalizing the tangential velocity improves in all cases the performances of the methods. In particular, for the characteristic methods, this additional condition yield to a very accurate solution, while, without it, the method does not yields to a satisfactory approximation. Secondly, the results show how the penalization methods depend on the stabilization parameters, as well as the minimal values allowed in order to avoid instability. We observe that in several cases, as anticipated in Section 3, a stable solution

DOI: 10.1002/cnm.2918

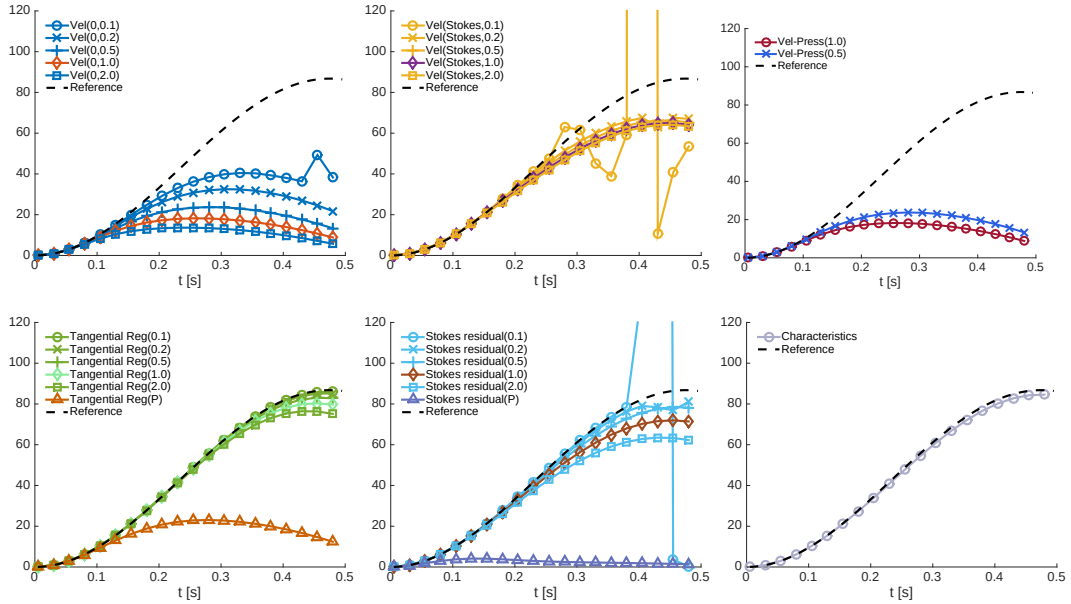

Figure 5. Benchmark 1 (full backflow), blood regime, penalizing the tangential velocity on the open boundary: incoming flow rate [cm^2/s] over time [s].

can be obtained also choosing a stabilization parameter smaller than the choice recommended in literature. Thirdly, both velocity and gradient penalizations with corrective terms resulted to be less robust with respect to the stabilization parameters than their counterpart without any correction. Finally, the results also allow to highlight some important similarities and differences between methods. In particular, the velocity penalization (without corrective term) for $\beta = 1$ and $\beta = 2$, and the velocity-pressure stabilization deliver very similar results, tending to excessively control the incoming flow after a certain threshold (about 20 cm^3/s). On the contrary, the gradient penalization methods (in particular the tangential regularization) allow a better approximation of the flow rate also when the incoming flow increases. However, it is worth noticing that the tangential regularization with stabilization parameter equal to the squared Poincaré constant (denoted by TANGENTIAL REG(P) in the legends) yields results very similar to the velocity penalization with $\beta = 1$ (both values assuring theoretical stability).

DOI: 10.1002/cnm.2918

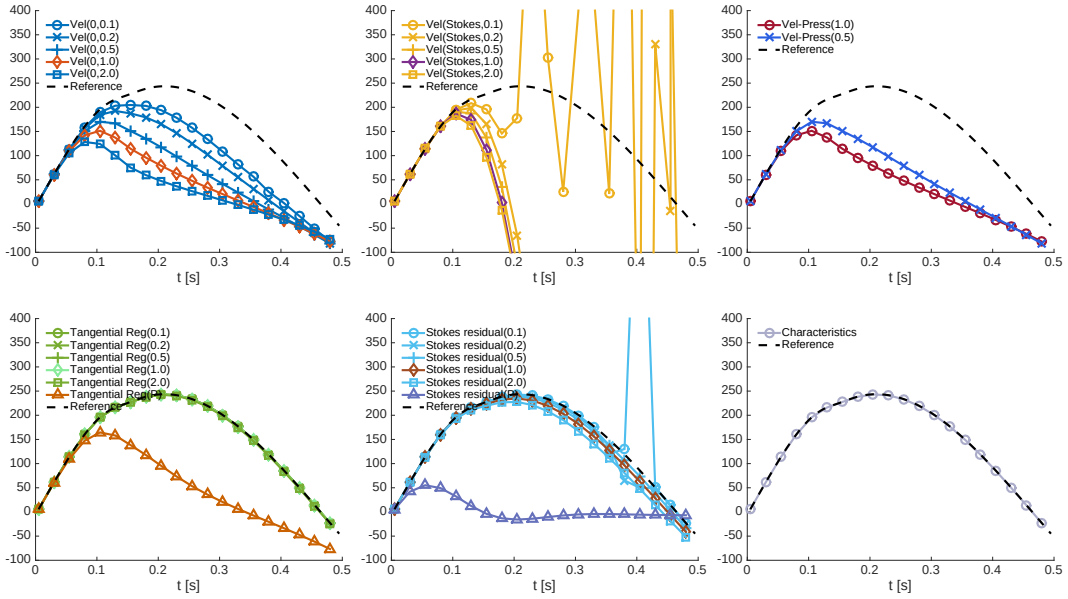

Figure 6. Benchmark 1 (full backflow), blood regime: average pressure drop [dyn/cm^2] over time [s].

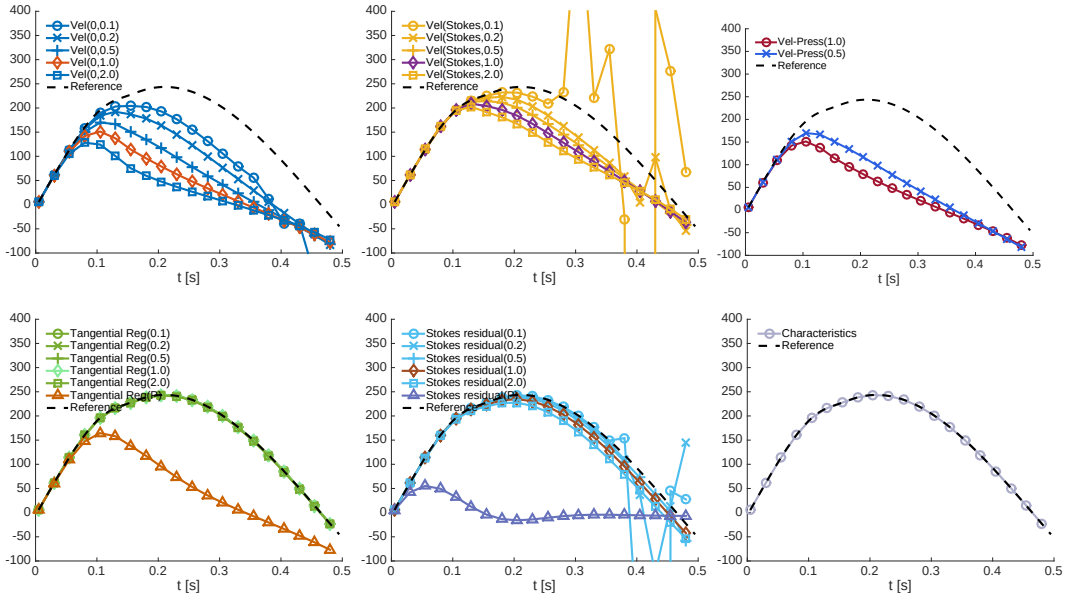

Figure 7. Benchmark 1 (full backflow), blood regime, penalizing the tangential velocity on the open boundary: average pressure drop [dyn/cm^2] over time [s].

As next, we compare more in details the solution profile on the open boundary at $t = 0.48$ (peak backflow). The results are shown in Figures 8-9 (normal velocity profiles) and 10-11 (pressure).

For the velocity and gradient penalizations, for the sake of clarity, only the results for selected choices are shown. In particular, for VEL($\mathbf{u}_0, \beta$) we consider the results for $\beta = 1.0$ (which assures stability) and for the lowest value of β yielding stable results ($\beta = 0.2$).

For TANGENTIAL REG(γ_0) we choose $\gamma_0 = 1.0$ (recommended in the literature), γ_0 so that $\gamma_0 \frac{h^2}{3}$ is equal to the squared Poincaré constant of the open boundary, and the lowest value of

DOI: 10.1002/cnm.2918

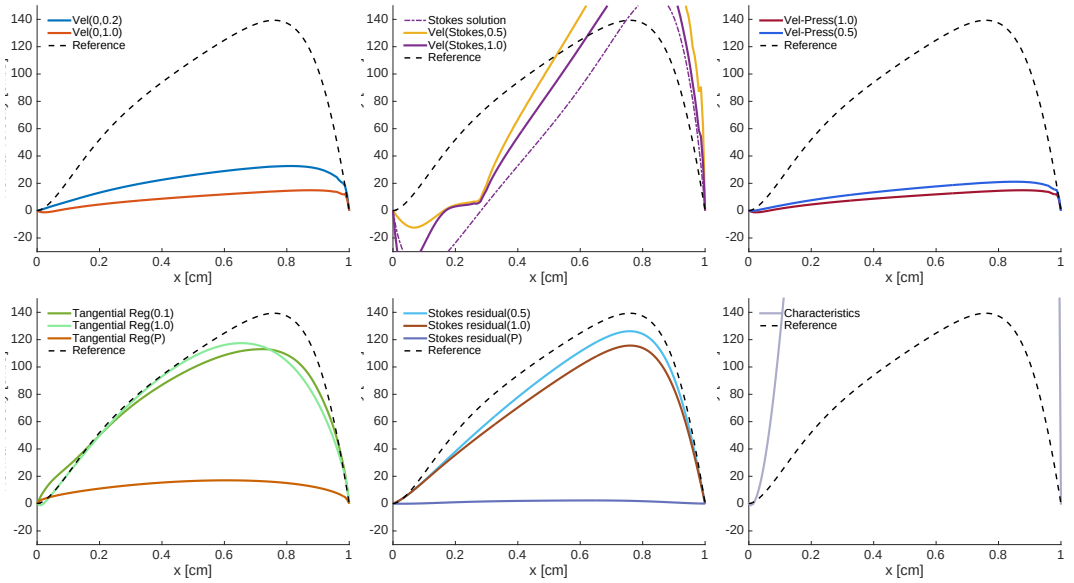

Figure 8. Benchmark 1 (full backflow), blood regime (time $t = 0.48$ s): Normal velocity profiles along the open boundary [cm/s].

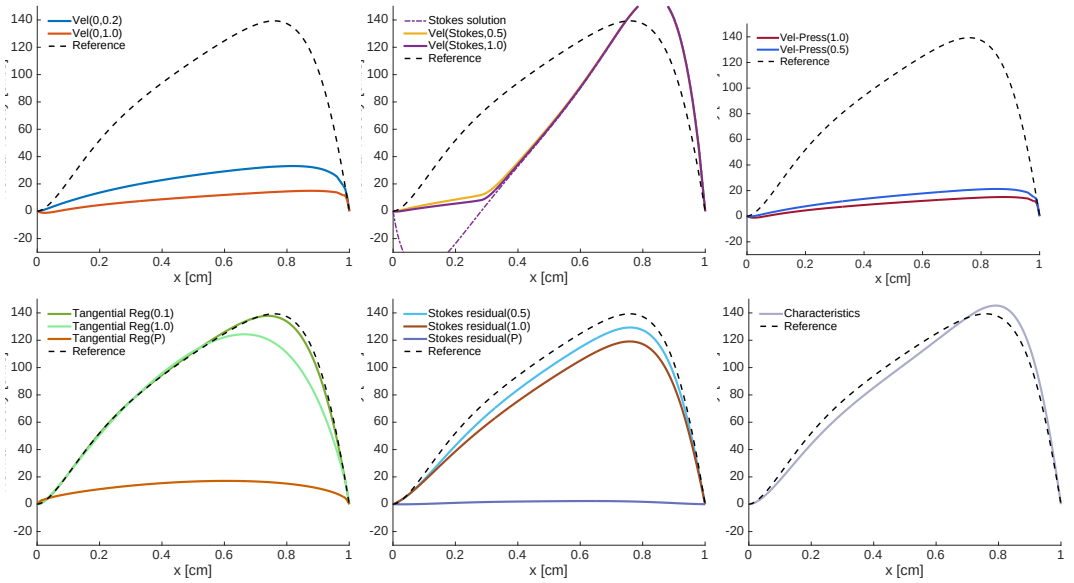

Figure 9. Benchmark 1 (full backflow), blood regime, penalizing the tangential velocity on the open boundary (time $t = 0.48$ s): Normal velocity profiles along the open boundary [cm/s].

γ_0 yielding stable results ($\gamma_0 = 0.1$). Similar choices will be considered also for the the method Stokes Residual(σ_0).

The results show that the velocity penalization methods are very sensitive to the corrective profile, even decreasing the stabilization parameter. The latter, in particular, yields a flattening of the velocity profile when the corrective profile is set to zero. For the velocity penalization based on the Stokes solution, while the velocity profile tends to adapt to this corrective profile, one obtain very large errors in pressure. On the contrary, in gradient penalization approaches the assumptions on the corrective profiles have less influence, yielding overall more accurate results.

DOI: 10.1002/cnm.2918

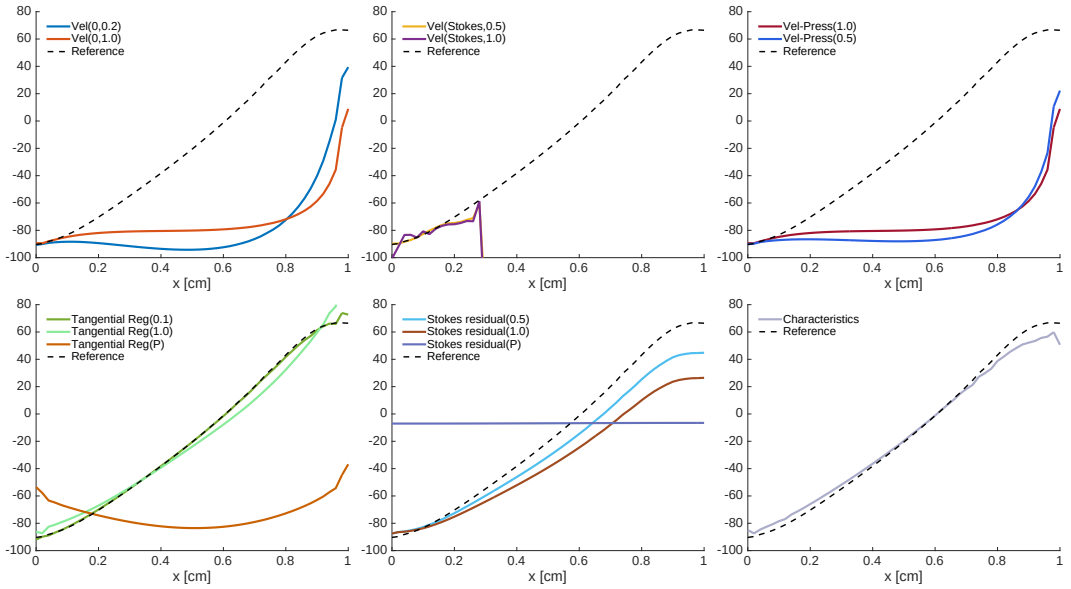

Figure 10. Benchmark 1 (full backflow), blood regime (time $t = 0.48$ s): Pressure profiles along the open boundary [dyn/cm^2].

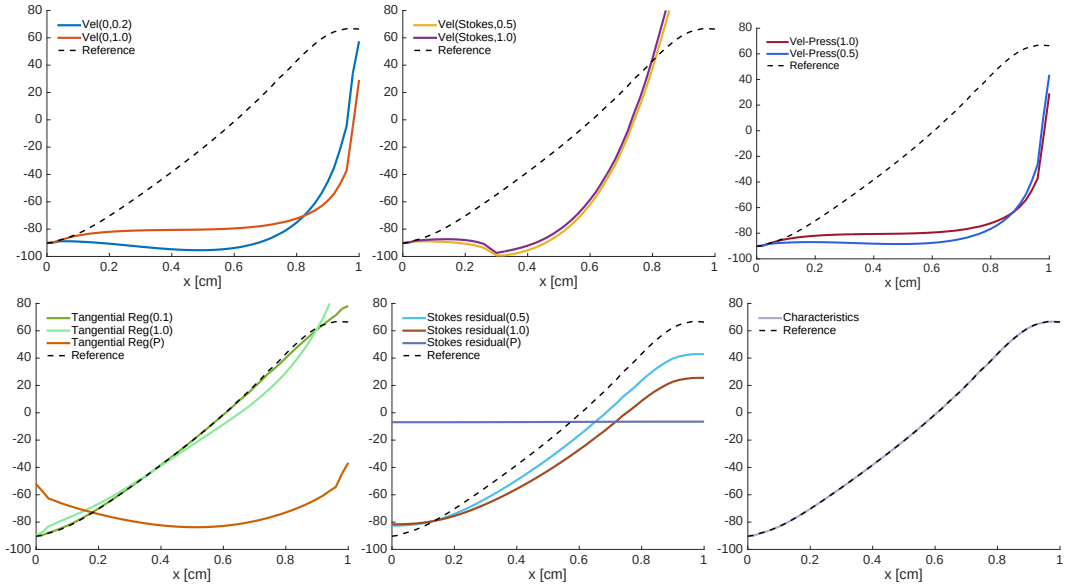

Figure 11. Benchmark 1 (full backflow), blood regime, penalizing the tangential velocity on the open boundary (time $t = 0.48$ s): Pressure profiles along the open boundary [dyn/cm^2].

4.5. Numerical results for respiratory regime

The second set of numerical tests considers the respiratory regime, setting the physical parameters as

$$\rho = 0.0012\,\mathrm{g/cm^3},\ \mu = 0.000185\,\mathrm{Poise},\ \Delta P = 2\,\mathrm{bary/cm}\ (\approx 0.0015\,\mathrm{mmHg/cm}),\ \omega = \frac{\pi}{2}\,\mathrm{rad/s}\,.$$

In this case, the choice of ω is motivated by the typical length of a breathing cycle (about 4 seconds). The peak Reynolds number amounts to 5190.

DOI: 10.1002/cnm.2918

Figure 12 shows the corresponding reference solutions for velocity and pressure at peak backflow instants, computed with mesh characteristic size $h = 0.02$ cm and time step $\delta t = 0.01$ s. and $t = 0.95$ s.

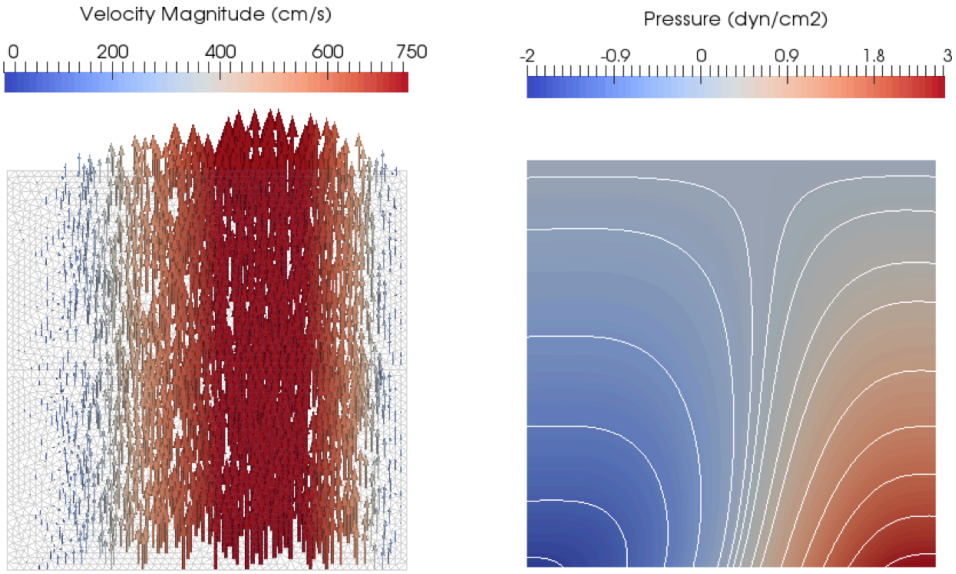

Figure 12. Reference solution (Benchmark 1, air) at peak backflow in air regime (t=0.95 s). Left: Mesh and glyph vector of the velocity field. Right: Pressure isolines.

As a validation of the finite element solver, we solve first the backflow problem using a velocity penalization method (with boundary condition modified as in (11)) with $\boldsymbol{u}_0 = \boldsymbol{u}_{\text{ref}}$, and the results are shown in Figure 13.

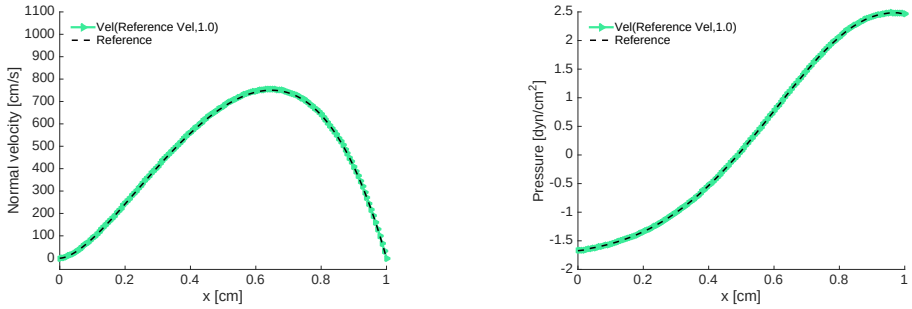

Figure 13. Profiles of velocity (left) and pressure (right) at the inflow boundary (peak backflow, $t = 0.95$ s), using an open boundary stabilization based on a velocity penalization towards the reference velocity (Benchmark 1, air regime).

Figures 14-15 and Figures 16-17 show the incoming flow rate and the average pressure drop, respectively, considering several stabilization methods and different choices of the parameter values. In particular, Figures 15 and 17 refer to the results including the additional constraint on vanishing tangential velocity to zero on the open boundary.

The observations made in the case of the blood flow regime are mostly confirmed in the respiratory case. In particular, the velocity penalization methods without corrective profiles tend to limit the incoming flow (up to about 40 cm^3/s), similarly to the case of velocity-pressure stabilization. Using a corrective profile based on a Stokes solution allows larger incoming flow, resulting however in inaccurate pressure drops. The gradient penalization methods deliver in general more accurate profiles, with a slightly worse accuracy than in the blood flow regime.

DOI: 10.1002/cnm.2918

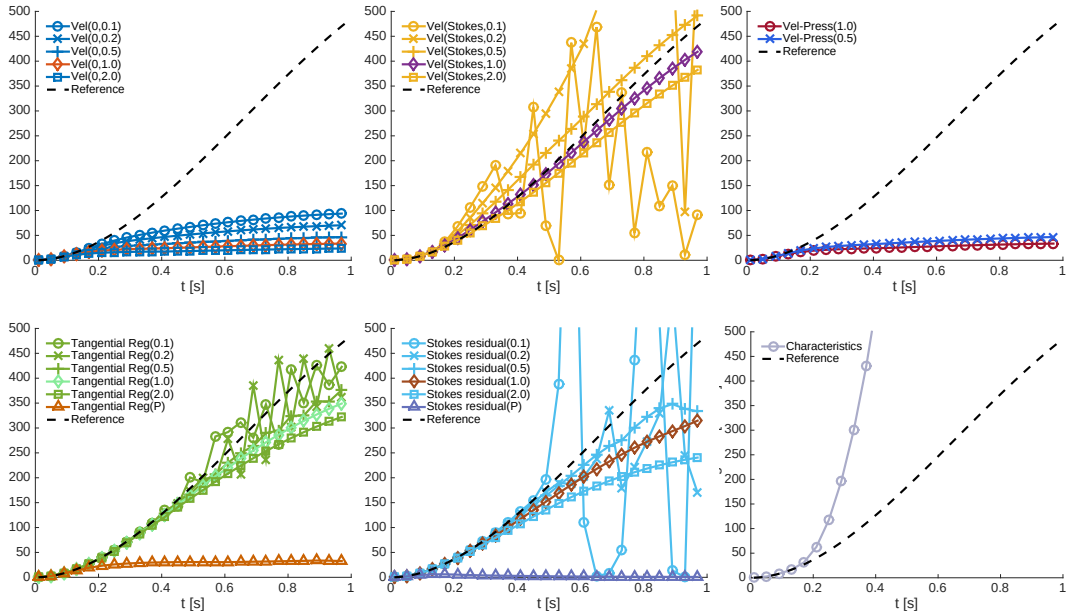

Figure 14. Benchmark 1 (full backflow), air regime: incoming flow rate [cm^2/s] over time [s].

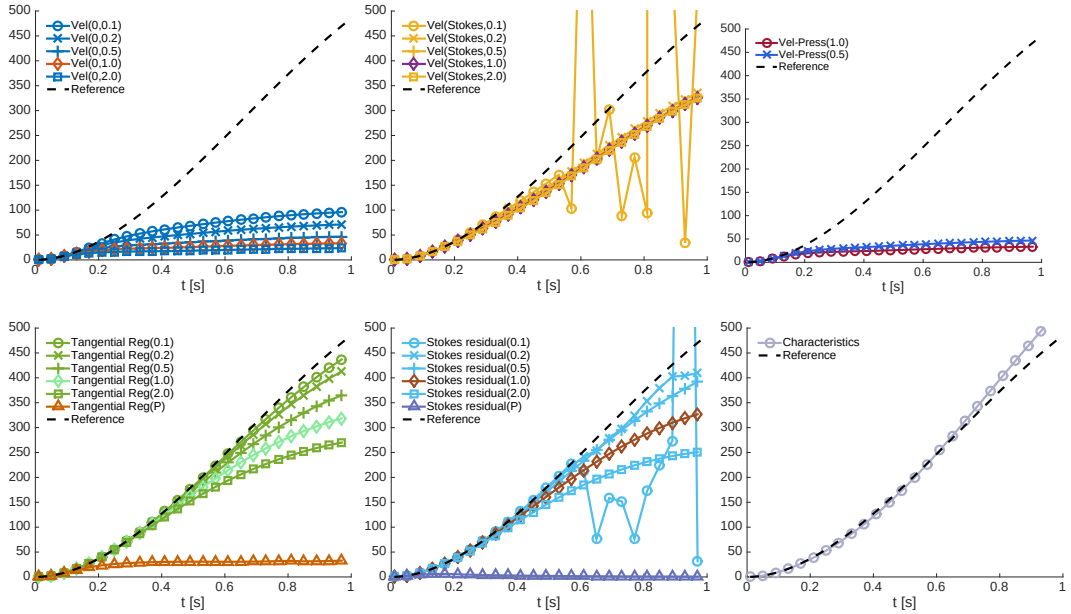

Figure 15. Benchmark 1 (full backflow), air regime, penalizing the tangential velocity on the open boundary: incoming flow rate [cm^2/s] over time [s].

Finally, the results confirm that the recommended values for $\beta = 1$, $\gamma_0 = 1$, $\sigma_0 = 1$ (in the respective methods) deliver stable results.

The detailed normal velocity and pressure profiles at time $t = 0.95$ s (peak backflow) are shown for all stabilization methods following the notation from Section 3.5 in Figures 18-19 and 20-21, respectively. As before, for VEL($\mathbf{u}_0, \beta$) we consider the results for $\beta = 1.0$ (which assures stability) and for the lowest value of β yielding stable results. Similar choices have been made for TANGENTIAL REG(γ_0) (choosing $\gamma_0 = 1.0$, γ_0 so that $\gamma_0 \frac{h^2}{3}$ is equal to the squared

DOI: 10.1002/cnm.2918

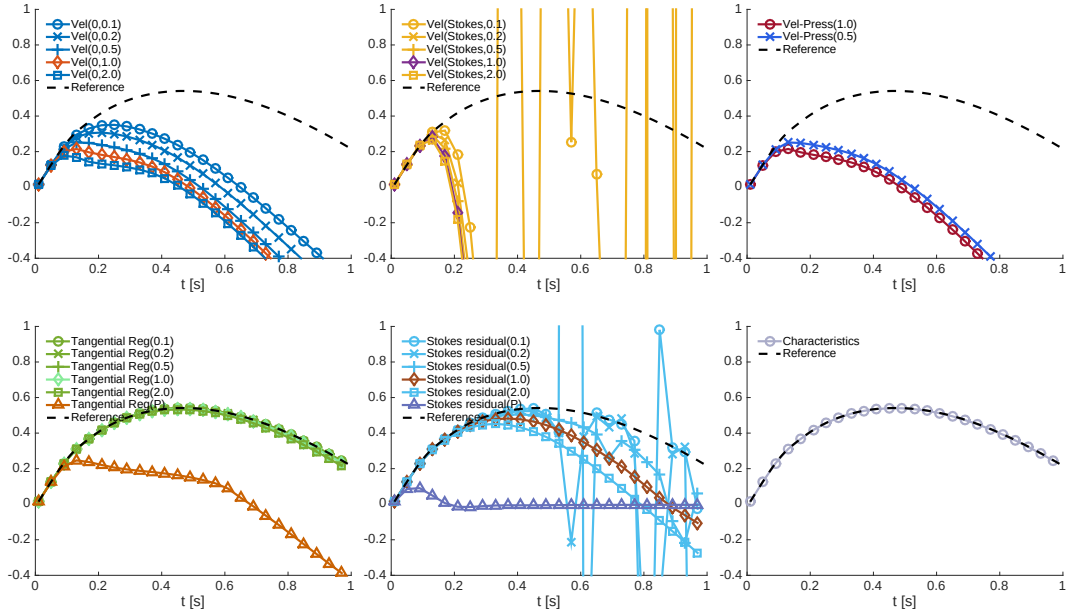

Figure 16. Benchmark 1 (full backflow), air regime: Average pressure drop [dyn/cm^2] over time [s].

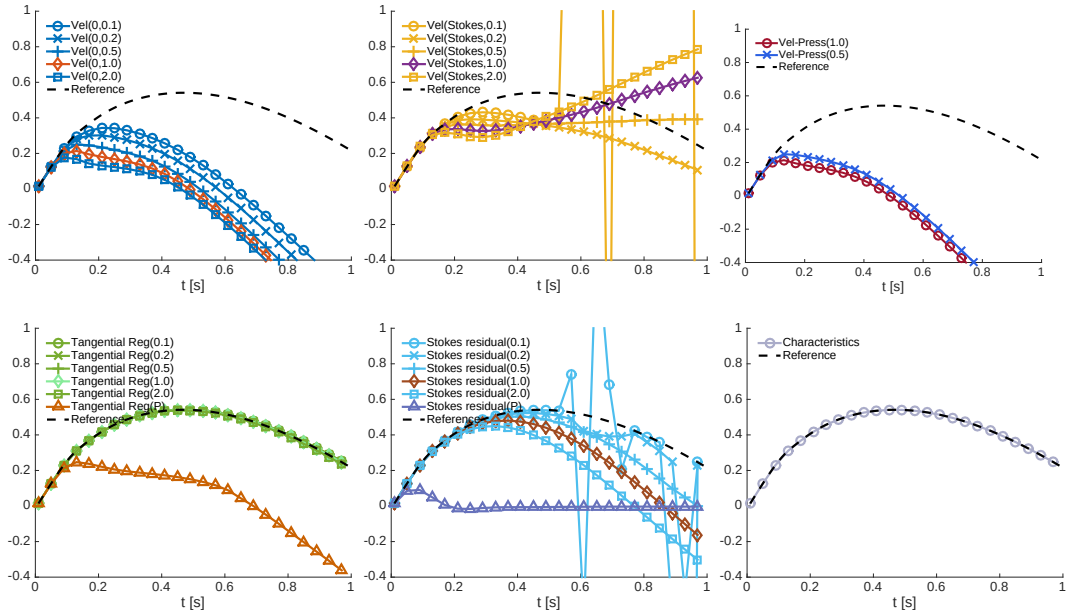

Figure 17. Benchmark 1 (full backflow), air regime, penalizing the tangential velocity on the open boundary: Average pressure drop [dyn/cm^2] over time [s].

Poincaré constant of the open boundary, and the lowest value of γ_0 yielding stable results) and for the method Stokes Residual(σ_0).

The results confirm that the velocity penalization methods are very sensitive to the corrective profile, even decreasing the stabilization parameter. The gradient penalization approaches deliver more accurate profiles. However, the accuracy of the approximation is poorer than the blood flow regime. As for the blood flow regime, the method of characteristics yield satisfactory

DOI: 10.1002/cnm.2918

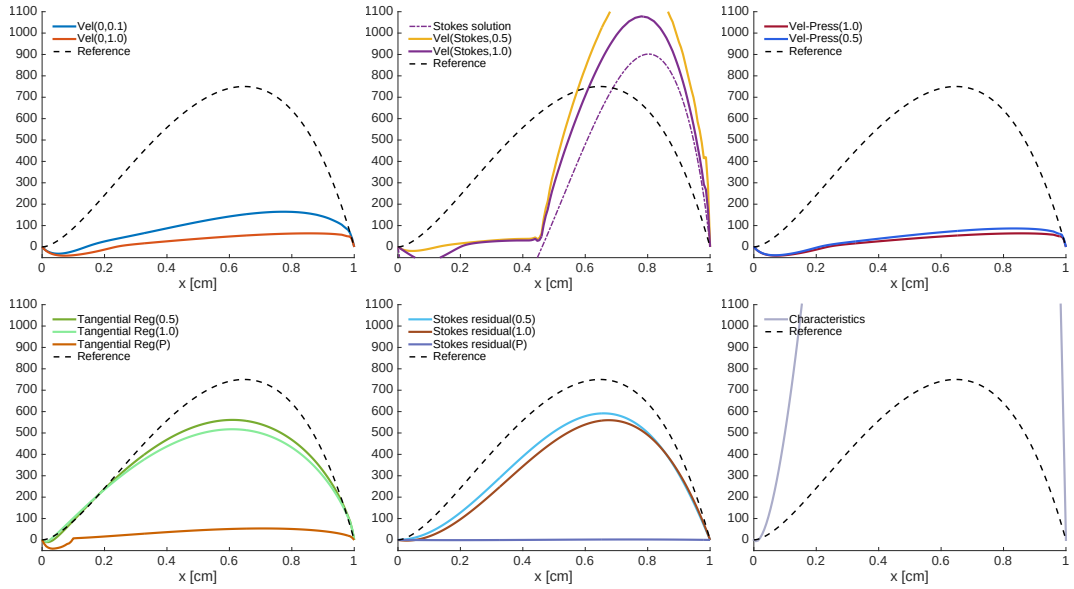

Figure 18. Benchmark 1 (full backflow), air regime (time $t = 0.95$ s): Normal velocity profiles along the open boundary [cm/s].

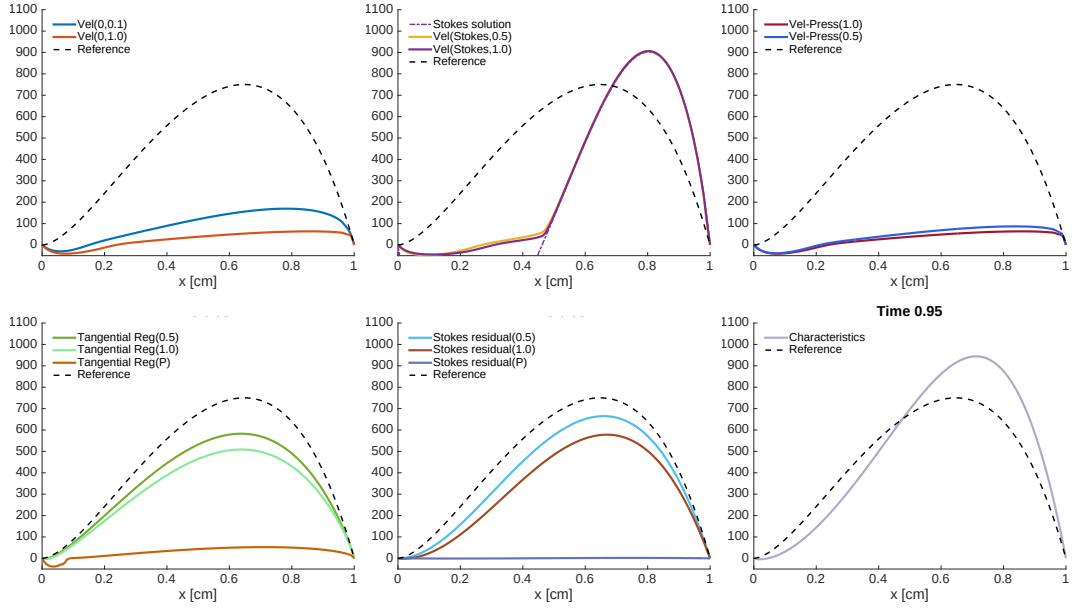

Figure 19. Benchmark 1 (full backflow), air regime, penalizing the tangential velocity on the open boundary (time $t = 0.95$ s): Normal velocity profiles along the open boundary [cm/s].

results only including the additional condition on vanishing tangential velocity, achieving, in this case, an accuracy similar to the tangential regularization.

DOI: 10.1002/cnm.2918

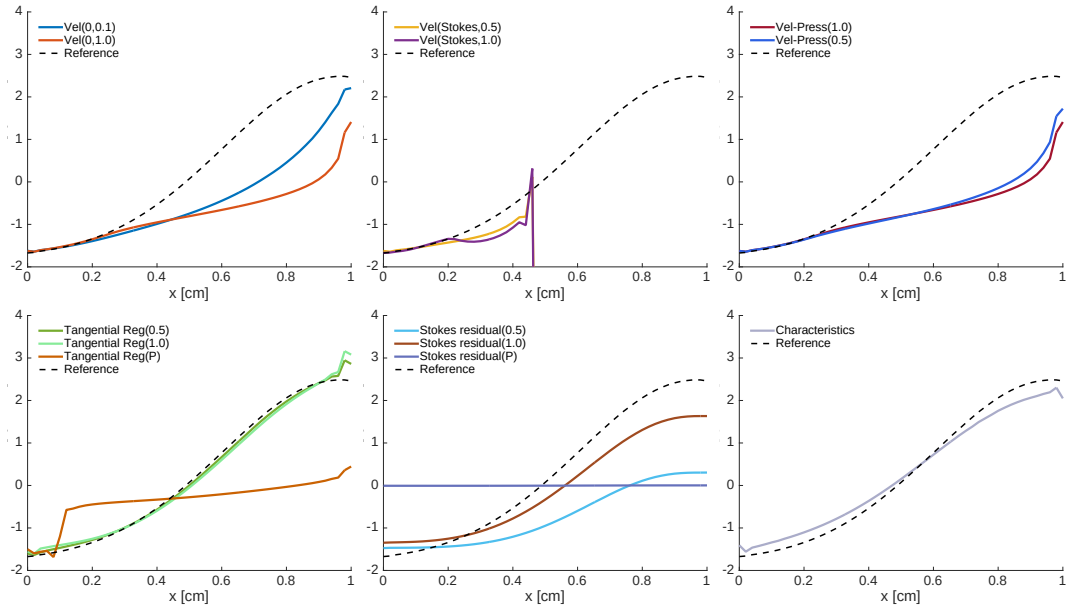

Figure 20. Benchmark 1 (full backflow), air regime (time $t = 0.95$ s): Pressure profiles along the open boundary [dyn/cm^2].

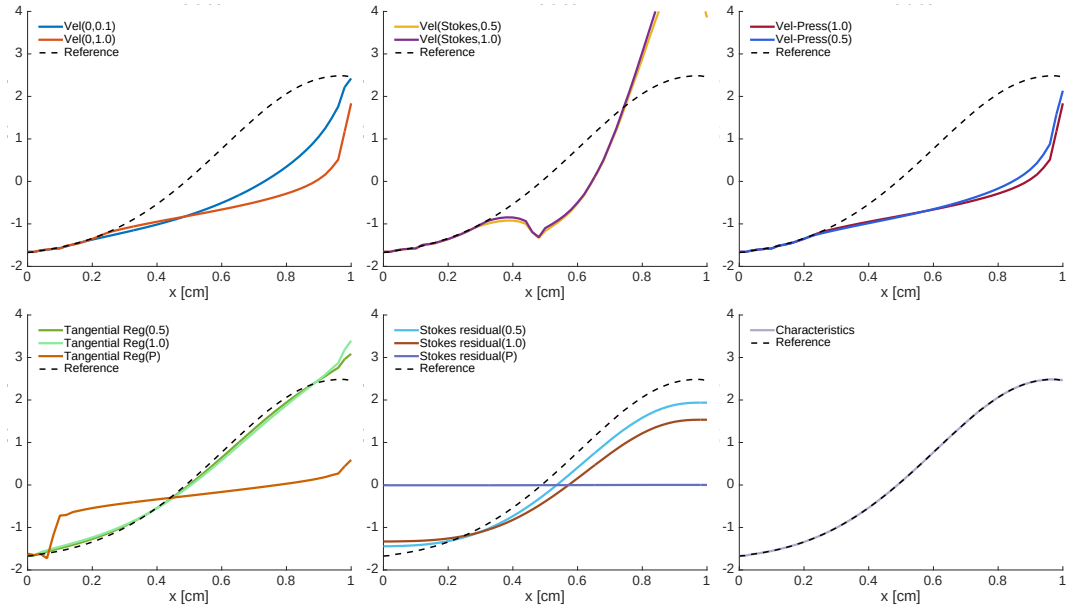

Figure 21. Benchmark 1 (full backflow), air regime, penalizing the tangential velocity on the open boundary (time $t = 0.95$ s): Pressure profiles along the open boundary [dyn/cm^2].

4.6. Discussion

In this benchmark, characterized by a full flow reversal on the open boundary, the gradient-penalization methods resulted the most accurate in both regimes, while velocity penalization failed to reproduce flow dynamics for large backflow (without a corrective velocity profile) or yielded unphysical pressure (employing a corrective profile based on the solution of a Stokes problem).

In more details, the performance of each method can be summarized as follows.

DOI: 10.1002/cnm.2918

- **Velocity penalization approach (without correction profile)**. The velocity penalization produces a flattening of the open boundary velocity profile at backflow, leading also to (small) discrepancies in the errors in the pressure profile.
- **Velocity penalization approach (with correction profile)**. Including a correction profile, in this case based on a Stokes flow, yields to an increased inflow rate compared with the case without correction, as the stabilized solution tends to match the correcting profile. Nevertheless, since this profile is still different from the reference one, both the errors in pressure and velocity remain large. Therefore, it is worth noticing that the results obtained with velocity penalization methods are in general very sensitive to the correcting profile. Further tests (not shown here) showed that the results clearly improve when the target profile is more symmetric (e.g. similar to a Womersley flow, consistently with the findings in [26]) or when the correcting profile is taken equal to the reference solution (see, e.g., Figures 3 and 13).
- **Velocity penalization + total pressure.** This methods yields similar results to the ones obtained with velocity penalization approach without correction profile. To some extend, this has to be expected given the particular setting of the benchmark in which the velocity on the open boundary is mostly normal, hence leading to a total pressure term similar to a velocity penalization. Note that, as observed in the presentation of the method, the total pressure term has been discretized semi-implicitly in time, hence not assuring a fully discrete energy balance. In our numerical test, this resulted (consistent with [2]) in the arise of spurious oscillations when increasing the value of β (results omitted).
- **Tangential derivative regularization**. This method resulted in the best performing one: it has a similar accuracy than the Stokes-residual method for the velocity but much more accurate in the pressures in blood and air regimes, for the recommended parameter value ($\gamma_0 = 1.0$). We remark that for the theoretical stabilization parameters, both velocity and gradient penalization methods (without correction) deliver similar results in these numerical examples.
- **Stokes-residual stabilization**. This method is the second best performing. One can obtain slightly better results in terms of the velocity compared with the tangential regularization, but worse results in terms of the pressure in the presented test cases. As mentioned in the text, it needs slightly larger parameter values than the tangential regularization to remain stable. This may be due to the fact that the corrective pressure gradient in the Stokes residual injects (controlled) energy but the stabilization is not able to compensate it if the parameter is not large enough. It is also remarkable that for theoretical stabilization parameter (squared Poincaré constant) the results are much worse than in the case of the tangential regularization.
- **Characteristics**. The numerical results in presence of full flow reversal, including the homogeneous boundary condition on the tangential velocity on the open boundary, are encouraging. However, the performance might be biased by the fact that the additional boundary condition is, in this particular case, consistent with the reference velocity. If this constraint is not set, the method does not deliver accurate results.

5. BENCHMARK 2: CHANNEL WITH ASYMMETRIC STENOSIS

The goal of the second test is to assess and compare the stabilization methods when backflow arises on a subset of the open boundary, e.g., in the presence of recirculation regions due to vortex propagation.

5.1. Benchmark setting

We consider the two computational domains Ω and Ω_{ext} depicted in Figure 22, describing two channels of lentghs L_S and L_{ext} with an asymmetric stenosis (obstruction). Namely, the

DOI: 10.1002/cnm.2918

lateral boundary is parametrized via

$$\Gamma_{\mathrm{S},i} = \left\{ (x,y) \mid y = c_i, \overbrace{\text{for } x \in [0,a] \cup [b,L]}^{\text{straight wall}}, \right. \\ \left. y(x) = c_i + d_i \exp\left(1 - \left(\frac{4(b-x)(x-a)}{(b-a)^2} + \epsilon\right)^{-2}\right), \underbrace{\text{for } x \in [a,b]}_{\text{stenosis}} \right\} \tag{31}$$

with $a = 0.15$ cm and $b = 0.6$ cm, and $c_1 = R$, $d_1 = -0.35$ and $c_2 = 0$, $d_2 = 0.25$ for the upper ($i = 1$) and lower ($i = 2$) boundary, respectively (see Figure 22 for details), and $\epsilon = 10^{-7}$. Moreover, the length is set to $L = L_S = 1.5$ cm for the shorter channel Ω and to $L = L_{\mathrm{ext}} = 3.5$ cm for the extended channel Ω_{ext}.

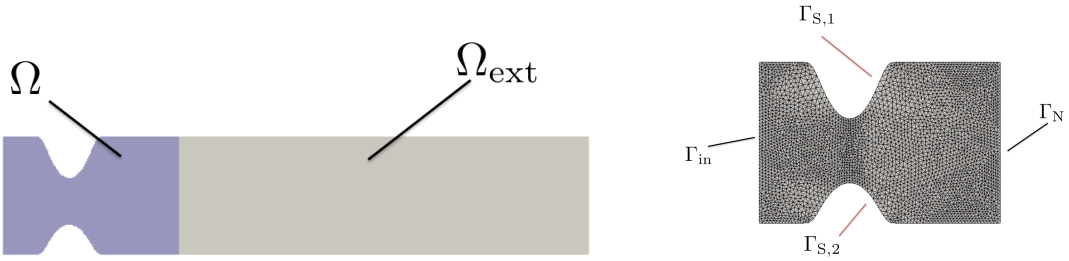

Figure 22. Left: The domains Ω_{ext} and Ω considered for this benchmark (blood regime). Right: The shorter domain Ω with the considered spatial discretization and the partition of the boundary.

The Navier–Stokes equations are first solved on Ω_{ext} in order to generate a reference solution, which will be stable as long as the vortices do not reach the open boundary Γ_N^{ext}. Namely, we consider the following boundary conditions:

$$\begin{cases} \boldsymbol{u}_{\mathrm{ref}} = \boldsymbol{u}_{\mathrm{in}} & \text{on} \quad \Gamma_{\mathrm{in}}, \\ \boldsymbol{u}_{\mathrm{ref}} = \boldsymbol{0} & \text{on} \quad \Gamma_{\mathrm{S},1} \cup \Gamma_{\mathrm{S},2}, \\ \boldsymbol{\sigma}(\boldsymbol{u}_{\mathrm{ref}}, p_{\mathrm{ref}})\boldsymbol{n} = \boldsymbol{0} & \text{on} \quad \Gamma_N^{\mathrm{ext}} \end{cases} \tag{32}$$

Then, the benchmark problem is defined on the shorter domain Ω, applying the load computed for the extended geometry as a Neumann boundary condition on the open boundary:

$$\begin{cases} \boldsymbol{u}_{\mathrm{back}} = \boldsymbol{u}_{\mathrm{in}} & \text{on} \quad \Gamma_{\mathrm{in}}, \\ \boldsymbol{u}_{\mathrm{back}} = \boldsymbol{0} & \text{on} \quad \Gamma_{\mathrm{S},1} \cup \Gamma_{\mathrm{S},2}, \\ (\mu \boldsymbol{\nabla} \boldsymbol{u}_{\mathrm{back}} - p_{\mathrm{back}} \boldsymbol{1})\boldsymbol{n} = (\mu \boldsymbol{\nabla} \boldsymbol{u}_{\mathrm{ref}} - p_{\mathrm{ref}} \boldsymbol{1})\boldsymbol{n} & \text{on} \quad \Gamma_N, \end{cases} \tag{33}$$

The velocity boundary data $\boldsymbol{u}_{\mathrm{in}}$ on the boundary Γ_{in} is given by the Womersley solution (24).

This benchmark consists then of the following two steps:

- First, the extended domain is used to generate a reference stable solution so that the vortices take a considerable time to arrive to the open boundary Γ_N^{ext}. Namely, we solve the following Navier-Stokes problem: Find $\boldsymbol{u}_{\mathrm{ref}}(t) \in H^1(\Omega^{\mathrm{ext}})$, $p_{\mathrm{ref}}(t) \in L^2(\Omega^{\mathrm{ext}})$, for all $0 < t \leq T$, and Dirichlet boundary conditions $(32)_{1-2}$ such that

$$\begin{cases} \mathcal{A}(\boldsymbol{u}_{\mathrm{ref}}, \boldsymbol{v}) - \mathcal{B}(p_{\mathrm{ref}}, \boldsymbol{v}) = 0\,, \\ \mathcal{B}(q, \boldsymbol{u}_{\mathrm{ref}}) = 0 \end{cases} \tag{34}$$

  for all $\boldsymbol{v} \in H_0^1(\Omega^{\mathrm{ext}})$ and $q \in L^2(\Omega^{\mathrm{ext}})$.

DOI: 10.1002/cnm.2918

- Then, the benchmark problem is defined on the shorter domain, applying the load computed for the extended geometry as a Neumann boundary condition on the open boundary: Find $\boldsymbol{u}_{\text{back}}(t) \in H^1(\Omega)$, satisfying the Dirichlet boundary condition $(27)_2$, $p_{\text{back}}(t) \in L^2(\Omega)$, for all $0 < t \leq T$, and Dirichlet boundary conditions $(33)_{1-2}$, such that

$$\begin{cases} \mathcal{A}(\boldsymbol{u}_{\text{back}}, \boldsymbol{v}) - \mathcal{B}(p_{\text{back}}, \boldsymbol{v}) + \mathcal{S}_{\Gamma_N}(\boldsymbol{u}_{\text{back}}, \boldsymbol{v}) = (\mu \partial_{\boldsymbol{n}} \boldsymbol{u}_{\text{ref}} - p_{\text{ref}} \boldsymbol{n}, \boldsymbol{v})_{\Gamma_N}, \\ \mathcal{B}(q, \boldsymbol{u}_{\text{back}}) = 0 \end{cases} \tag{35}$$

  for all $\boldsymbol{v} \in H^1_0(\Omega)$ and $q \in L^2(\Omega)$. Naturally, the stabilization methods detailed in Section 3.5 are applied only on Γ_N.

Remark 2. *Notice that, in the setup of this benchmark, the backflow problem (33) could be also solved using a constant pressure on Γ_N, instead of the projection of the full tensor. That choice would still lead to recirculation regions convected through the open boundary. While a constant boundary pressure is the most common choice in applications to physiological flows, the corresponding numerical experiments (results omitted) showed that, using this boundary condition yields a numerical solution far from the reference one, even if the reference velocity is used as corrective term within a velocity penalization method. Hence, applying the full tensor on the Neumann boundary allows, in the context of this study, to perform a more detailed comparisons of the methods, avoiding additional errors due to the perturbation of the boundary load.*

5.2. Practical aspects of the benchmark setup

The numerical results have been computed following the steps detailed below. All the data needed to compute the numerical results shown in the following sections (meshes, boundary data, and simulation code) are available online[§].

Discretization. An unstructured triangular mesh of the unit square has been generated, specifying the mesh characteristic size h. The mesh has been created using FreeFem++.

Solution of extended (reference) problem A Navier-Stokes problem on Ω_{ext} with boundary conditions (32) has been solved (using FreeFem++).

Computation of boundary data With the chosen finite element spaces, the vector

$$\mathbf{T}_{\text{ref}} = (\mu \partial_{\boldsymbol{n}} \boldsymbol{u}_{\text{ref}} - p_{\text{ref}} \boldsymbol{n})$$

(where $\boldsymbol{n} = (0, 1)$ denotes the outgoing normal on Γ_{N}) has been computed, in order to impose the boundary condition on Γ_{N}.

As in the previous benchmark, the load in Problem (33) has been defined considering the L_2-projection of $\mathbf{T}_{\text{ref}}$ onto the space of piecewise linear function (using (30)), and applying as boundary condition $\hat{\mathbf{T}}_{\Gamma_{\text{N}}}$.

Solution of backflow problem A Navier-Stokes problem on the shorter domain Ω and boundary conditions (33) has been solved (using FreeFem++).

Evaluation The difference between the numerical solutions has been evaluated in terms of incoming flow $Q_{\text{in}}(\boldsymbol{u}) = \int_{\Gamma_{\text{N}}} \boldsymbol{u} \cdot \boldsymbol{n}$, average pressure drop

$$\Delta(p) = \frac{1}{|\Gamma_{\text{in}}|} \int_{\Gamma_{\text{in}}} p - \frac{1}{|\Gamma_{\text{N}}|} \int_{\Gamma_{\text{out}}} p$$

[§]See http://wias-berlin.de/people/caiazzo/backflow/.

DOI: 10.1002/cnm.2918

and, more in detail, monitoring the difference between the profiles on the inflow boundary Γ_N.

The temporal and spatial semi-discretizations are the same as for Benchmark 1 and are detailed in Section 4.2. As already mentioned above, the benchmark problem can be defined independently of the discretization (i.e., mesh, finite element spaces or time step) and of the numerical approximation of the boundary data (discretization of the inflow profile for the Dirichlet boundary and approximation of the load vector on the open boundary).

5.3. Numerical results for hemodynamics regime

The numerical tests are carried out considering a hemodynamics regime, i.e., setting the physical parameters as

$$\rho = 1.06\,\mathrm{g/cm^3},\ \mu = 0.035\,\mathrm{Poise},\ R = 1\,\mathrm{cm},\ \Delta P = 400\,\mathrm{bary/cm}\ (\approx 0.3\,\mathrm{mmHg/cm}),\ \omega = 2\pi\,\mathrm{rad/s}.$$

In this test case the peak Reynolds number turns to be 1817.

Figure 23 shows the numerical solutions in Ω for velocity and pressure at time t= 0.15 s, computed in the extended domain Ω_{ext} (mesh characteristic size $h = 0.02$ cm, time step $\delta t = 0.002$ s).

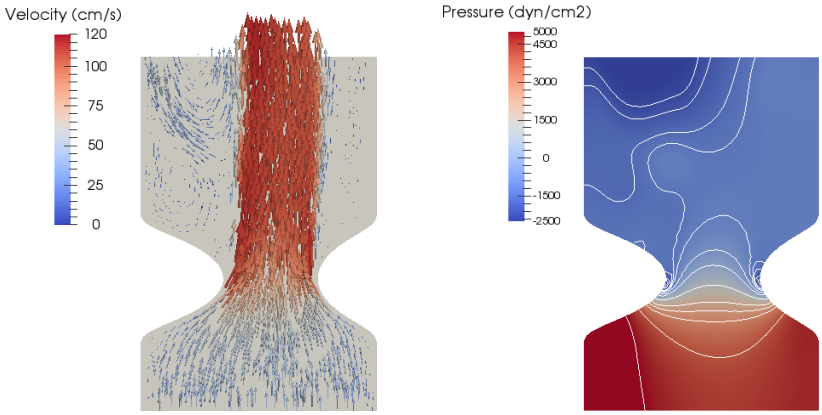

Figure 23. Benchmark 2 (stenosis), blood regime. Reference solution (computed in the domain Ω_{ext}, but visualized only in Ω) at time t=0.2 s. Left: Glyph vector of the velocity field. Right: Pressure field, including isolines.

As done for Benchmark 1, we solve the backflow problem using a velocity penalization method with $\boldsymbol{u}_0 = \boldsymbol{u}_{\mathrm{ref}}$, and the results are shown in Figure 24.

The curves in Figures 25 and 26 show the incoming flow rate and the average pressure drop, respectively, considering several stabilization methods and different choices of the parameter values.

In terms of these mean quantities, the best performing approaches appear to be the VEL($0,\beta$) followed by the TANGENTIAL REG(γ_0), which are both based on a zero corrective profile. The methods based on non-zero correcting profiles show a rather poor performance, an aspect that could be explained by the fact that the correcting profiles are very far from the target one. We also observe that the VEL-PRESS methods deliver very similar results to VEL($0,\beta$), with $\beta = 1$ and that the method of characteristics yields a solution that oscillates around the reference one. Notice that in this benchmark we did not impose a vanishing tangential velocity, as this condition is not consistent with the reference solution. In terms of the parameter values delivering stable results, the results in Figures 25 and 26 confirm the values found in the first benchmark.

As next, the detailed normal velocity and pressure profiles are compared with the reference solution considering two time steps (times $t = 0.20$ s and $t = 0.32$ s). The results for the

DOI: 10.1002/cnm.2918

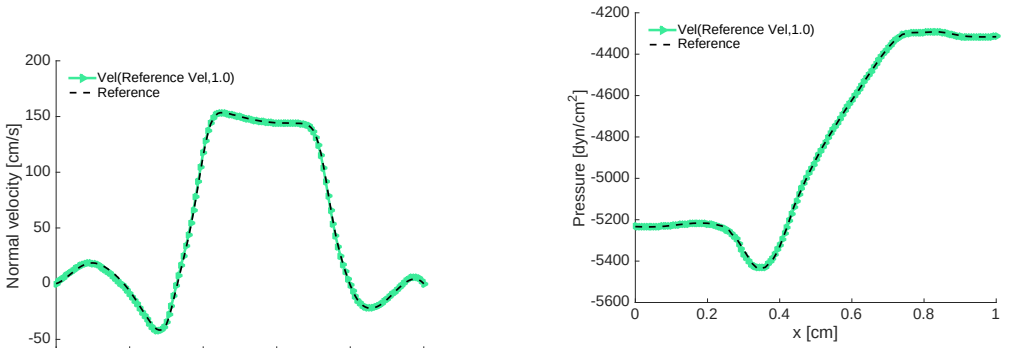

Figure 24. Benchmark 2 (stenosis), blood regime. Profiles of velocity (left) and pressure (right) on the open boundary at time $t = 0.2$ s, using an open boundary stabilization based on a velocity penalization towards the reference velocity.

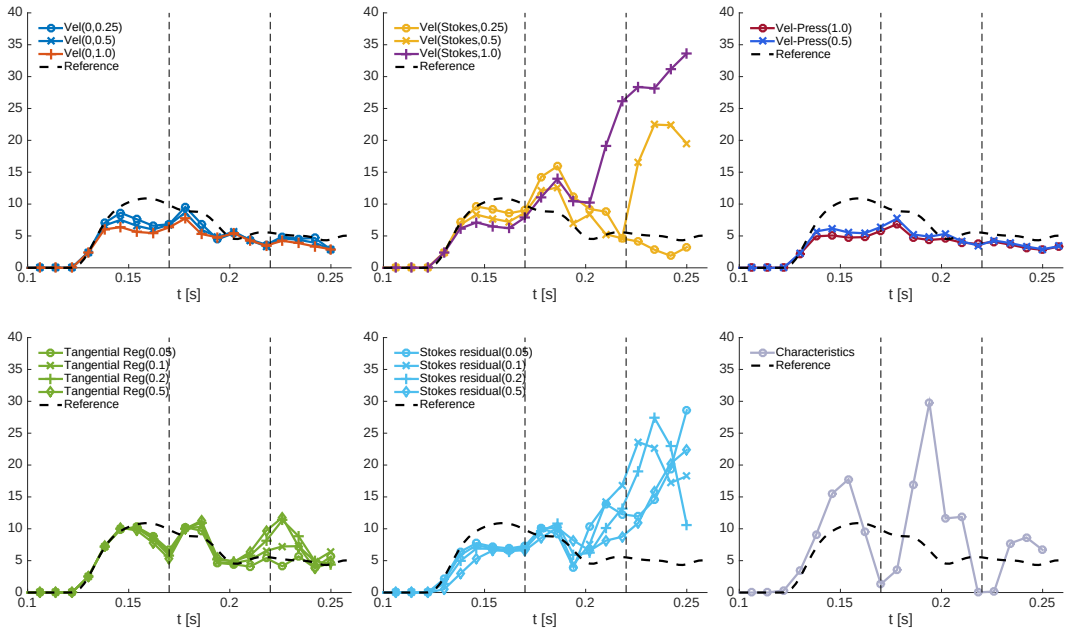

Figure 25. Benchmark 2 (stenosis), blood regime: incoming flow rate [cm^2/s] over time [s]. The curves are shown starting from $t = 0.10$ s. Before this instant, the different methods yield very similar results.

different stabilization methods (following the notation from Section 3.5) are shown in Figures 27–28 (for $t = 0.20$ s) and Figures 29–30 (for $t = 0.32$ s).

As for the previous benchmark, for VEL($\mathbf{u}_0, \beta$) we show the results for $\beta = 1$ and for the smallest value of β delivering stable results. Similarly, for TANGENTIAL REG(γ_0) and STOKES-RESIDUAL(σ_0) we show the results using the value of parameter assuring unconditional stability (squared Poincaré constant), the value recommended in literature ($\gamma_0 = \sigma_0 = 1$) and the minimal values delivering stable results.

The results confirm that the best performing approaches are the ones assuming a vanishing correcting profile. In particular, the VEL($\mathbf{0}, \beta$) resulted the most accurate. In particular, the superiority of this method appears related to the fact that, although it tends to flatten the velocity profile in the backflow regions, it introduces only a small perturbation of the *outflow* profile on the open boundary. In this setting where the backflow domain changes in time, the locality of the perturbation becomes very important in order to obtain a good solution.

DOI: 10.1002/cnm.2918

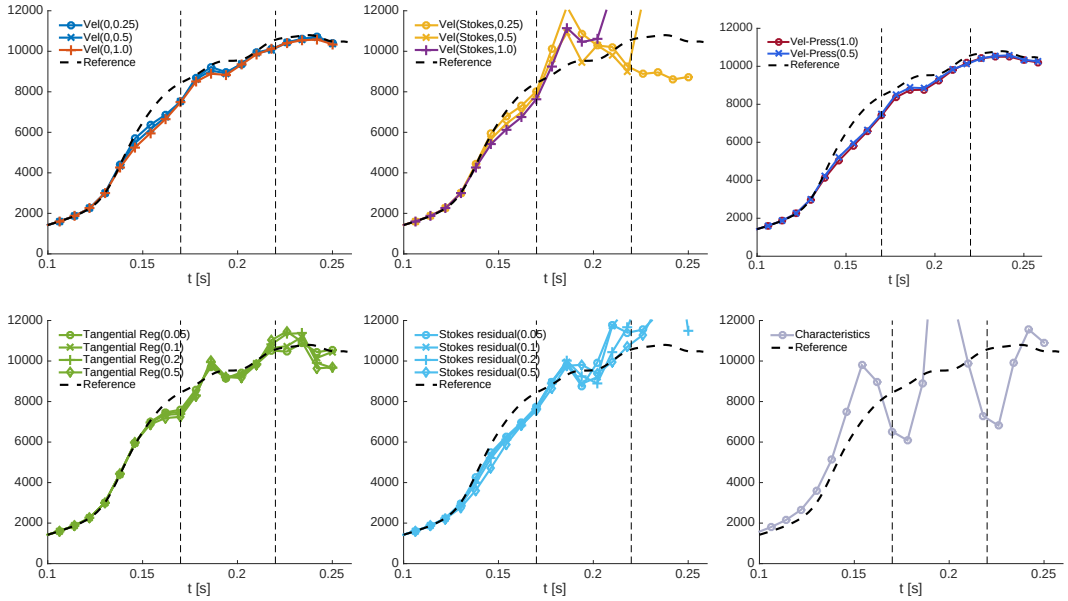

Figure 26. Benchmark 2 (stenosis), blood regime: Average pressure drop [dyn/cm^2] over time [s]. The curves are shown starting from $t = 0.10$ s. Before this instant, the different methods yield very similar results.

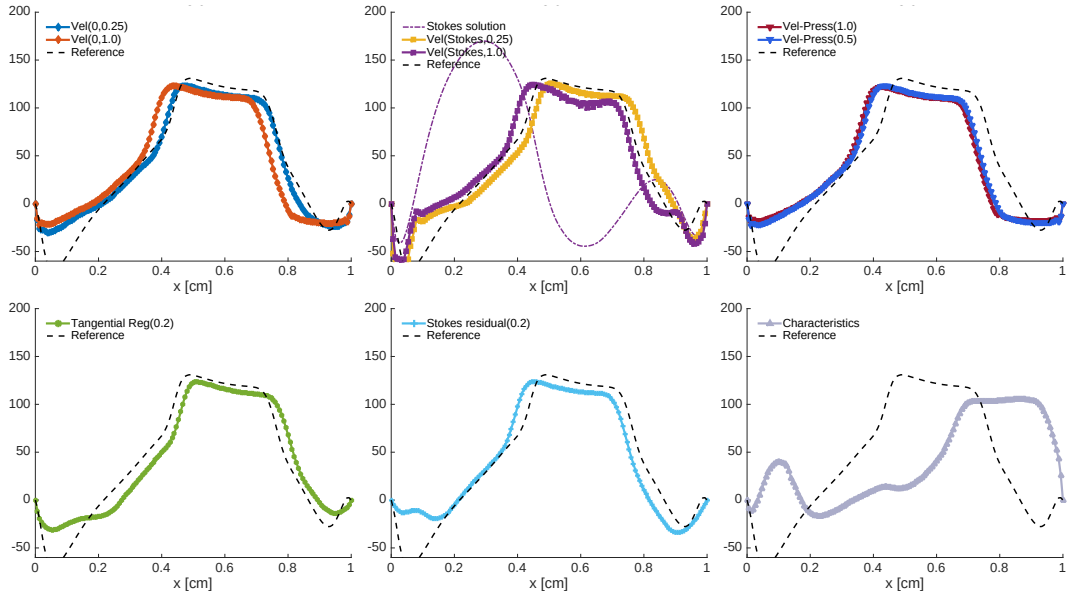

Figure 27. Benchmark 2 (stenosis), blood regime (time $t = 0.20$ s): Normal velocity profiles along the open boundary [cm/s].

The tangential regularization achieves (at time $t = 0.20$ s) a slightly better profile at backflow, but, at later times, it introduces a larger perturbation in the profile, which amount seems to depend on the choice of the parameter. This can be explained by the fact that the spatial derivatives used in the stabilization term introduce additional coupling of the degrees of freedom on the open boundary.

DOI: 10.1002/cnm.2918

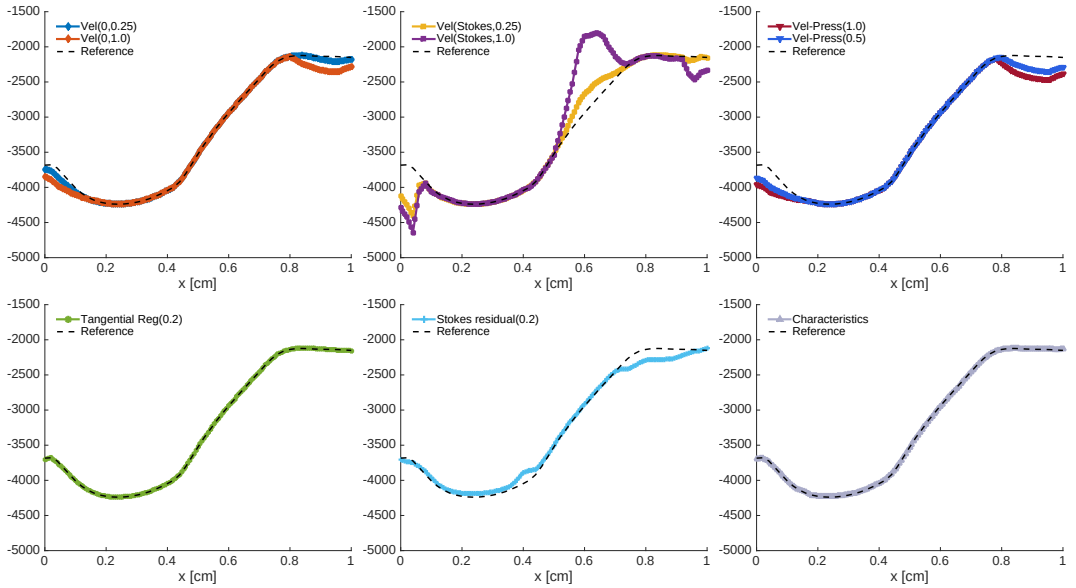

Figure 28. Benchmark 2 (stenosis), blood regime (time $t = 0.20$ s): Pressure profiles along the open boundary [dyn/cm^2].

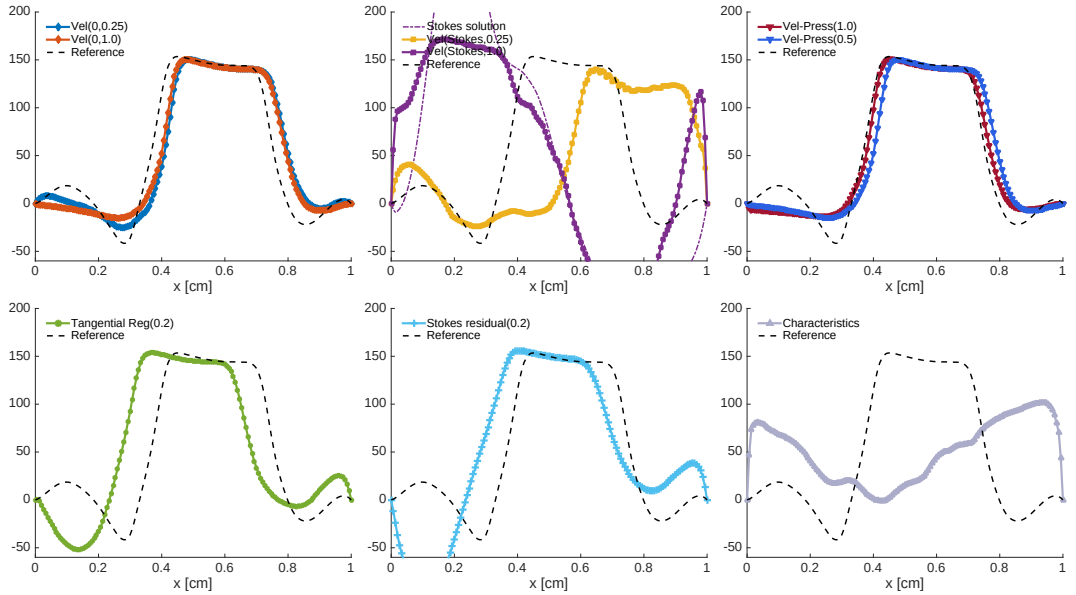

Figure 29. Benchmark 2 (stenosis), blood regime (time $t = 0.32$ s): Normal velocity profiles along the open boundary [cm/s].

5.4. Numerical results for respiratory regime

The second set of numerical tests considers the respiratory regime, setting the physical parameters as

$$\rho = 0.0012\,\mathrm{g/cm}^3,\ \mu = 0.000185\,\mathrm{Poise},$$

$$\Delta P = 2\,\mathrm{bary/cm}\ (\approx 0.0015\,\mathrm{mmHg/cm}),\ \omega = \frac{\pi}{2}\,\mathrm{rad/s},\ R = 1.5\,\mathrm{cm}.$$

With respect to the hemodynamics benchmark, the size R of the inlet boundary was increased, in order to reduce the peak velocity and hence the length of the extension required to generate the reference solution. The peak Reynolds number amounts to 1751.

DOI: 10.1002/cnm.2918

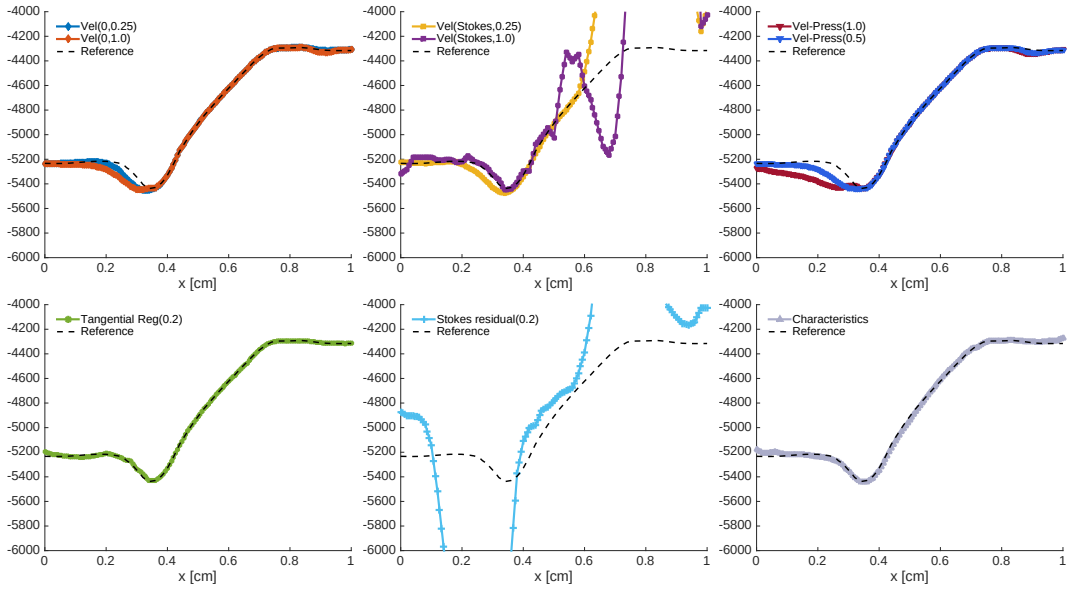

Figure 30. Benchmark 2 (stenosis), blood regime (time $t = 0.32$ s): Pressure profiles along the open boundary [dyn/cm^2].

Figure 31 shows the corresponding reference solutions for velocity and pressure at peak backflow instants, computed with mesh characteristic size $h = 0.015$ cm and time step $\delta t = 0.005$ s.

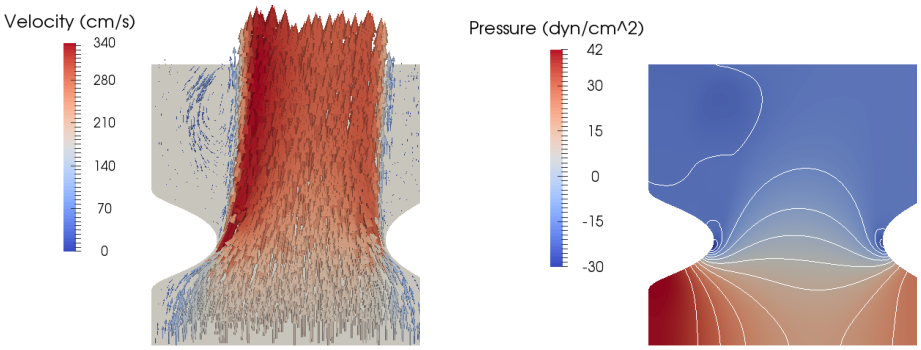

Figure 31. Benchmark 2 (stenosis), air regime. Reference solution at t=0.20 s. Left: Mesh and glyph vector of the velocity field. Right: Pressure isolines.

As a validation of the finite element solver, we solve first the backflow problem using a velocity penalization method with $\boldsymbol{u}_0 = \boldsymbol{u}_{\text{ref}}$, and the results are shown in Figure 32.

The curves in Figures 33 and 34 show the incoming flow rate and the average pressure drop, respectively, considering several stabilization methods and different choices of the parameter values.

All methods, except the method of characteristics, deliver acceptable solutions. In particular, the values of incoming flows remain close to the reference curve, while pressure drops are very accurately reproduced. In particular, it shall also be appreciated that, in this regime, the results of the methods (in terms of mean quantities) appear to be less sensitive to the stabilization parameters.

DOI: 10.1002/cnm.2918

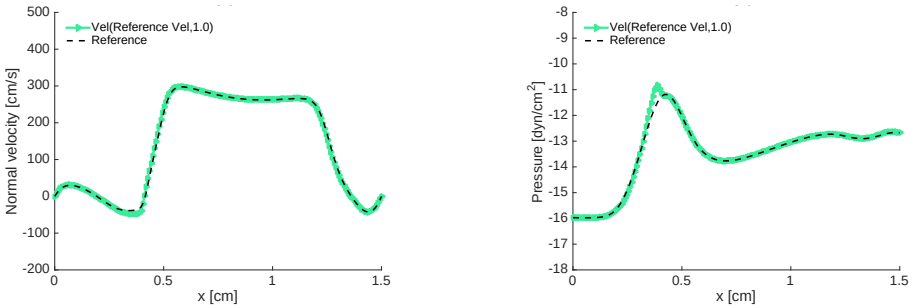

Figure 32. Profiles of velocity (left) and pressure (right) on the open boundary ($t = 0.20$ s), using an open boundary stabilization consistent with the reference velocity (Benchmark 2, air regime).

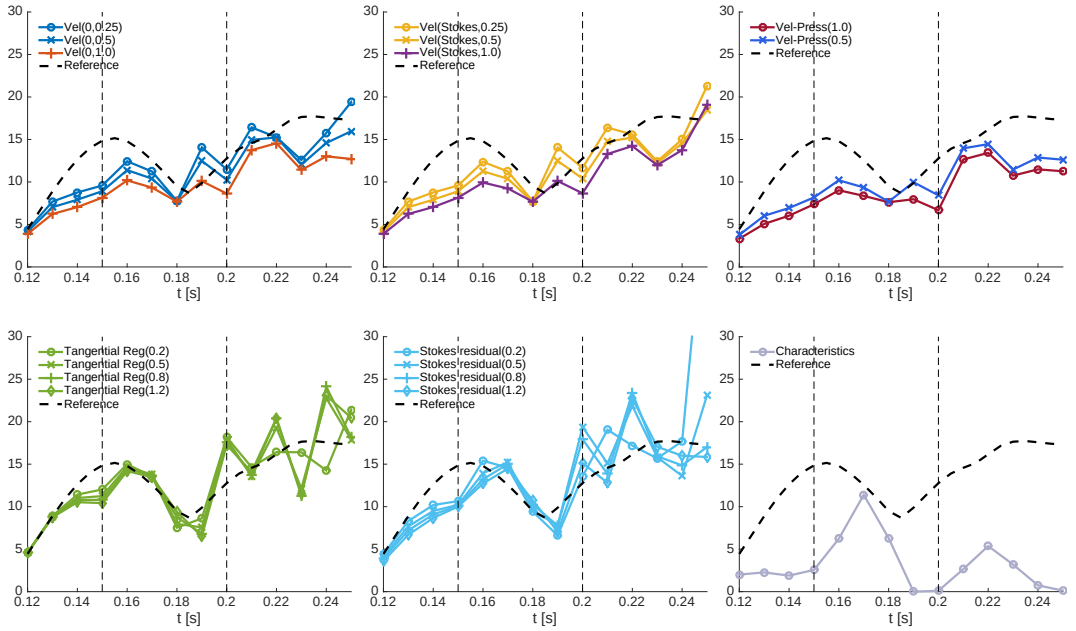

Figure 33. Benchmark 2 (stenosis), air regime: incoming flow rate [cm^2/s] over time [s]. The curves are shown starting from $t = 0.12$ s. Before this instant, the different methods yield very similar results.

DOI: 10.1002/cnm.2918

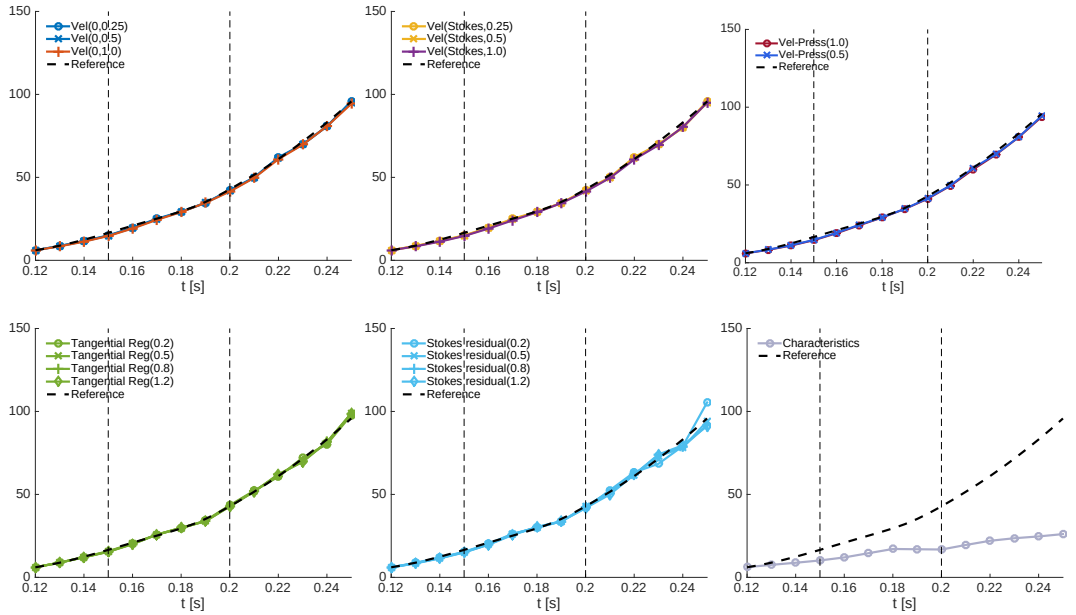

Figure 34. Benchmark 2 (stenosis), air regime: Average pressure drop [dyn/cm^2] over time [s]. The curves are shown starting from $t = 0.12$ s. Before this instant, the different methods yield very similar results.

DOI: 10.1002/cnm.2918

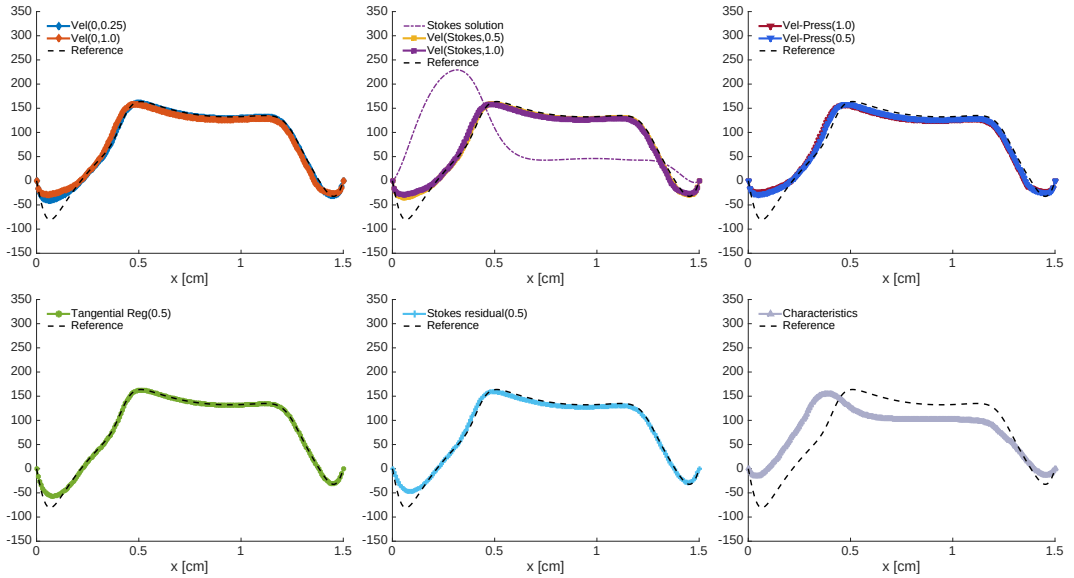

Figure 35. Benchmark 2 (stenosis), air regime (time $t = 0.15$ s): Normal velocity profiles along the open boundary [cm/s].

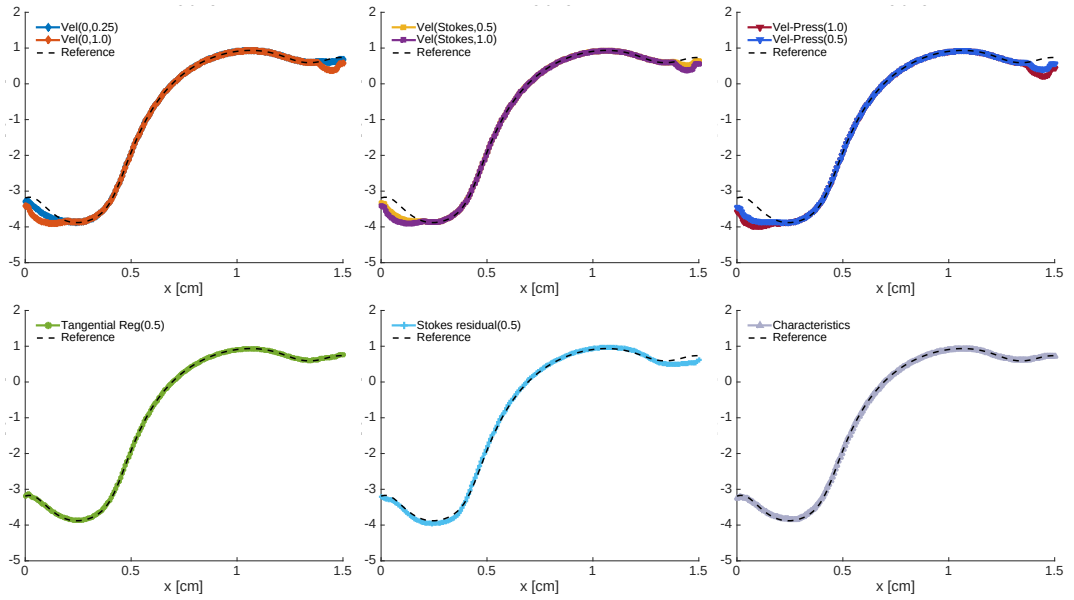

Figure 36. Benchmark 2 (stenosis), air regime (time $t = 0.15$ s): Pressure profiles along the open boundary [dyn/cm^2].

In order to provide a more detailed picture of the performance, the detailed normal velocity and pressure profiles at times $t = 0.15$ and $t = 0.20$ are shown, following the notation from Section 3.5, in Figures 35–38. As in the previous cases, for the penalization methods only selected curves are shown, focusing on the parameters assuring stability, the values recommended in literature, and on the minimal values delivering stable results. The results are considerably more accurate than in the blood regime. In particular, the tangential regularization yields the most accurate results at both considered time steps, by providing a good approximation of the velocity profile in the backflow parts of the open boundary and avoiding spurious oscillations in the pressure profile.

DOI: 10.1002/cnm.2918

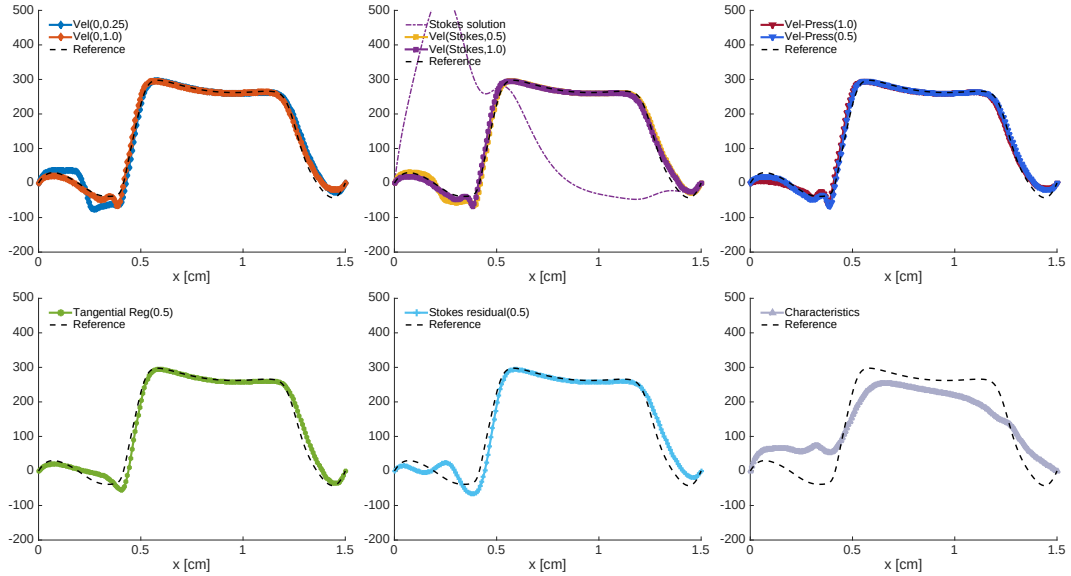

Figure 37. Benchmark 2 (stenosis), air regime (time $t = 0.2$ s): Normal velocity profiles along the open boundary [cm/s].

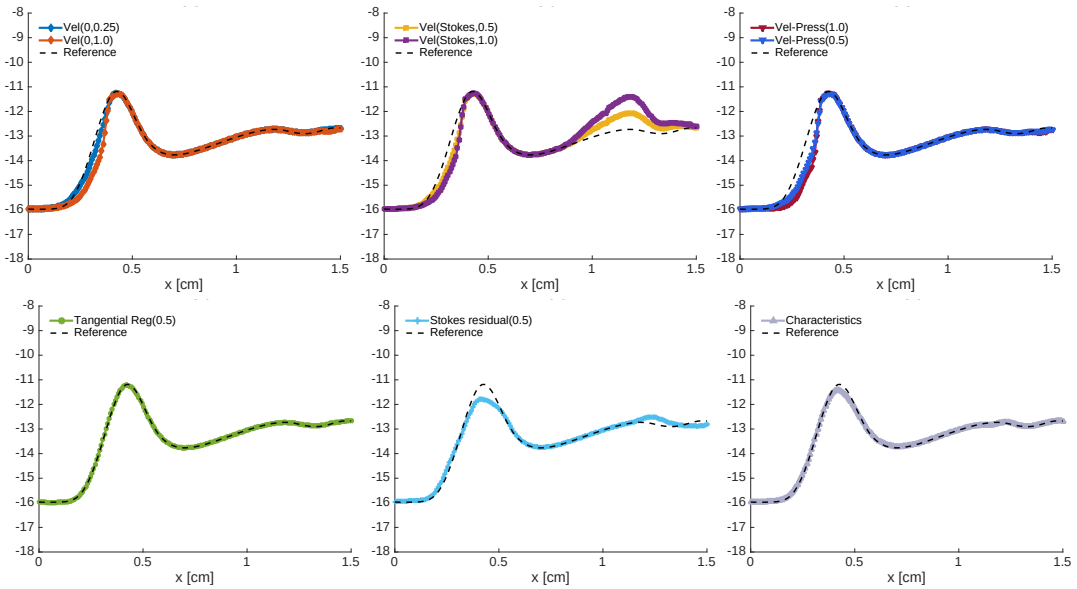

Figure 38. Benchmark 2 (stenosis), air regime (time $t = 0.2$ s): Pressure profiles along the open boundary [dyn/cm^2].

DOI: 10.1002/cnm.2918

5.5. Discussion

In the case of a vortex shield, when the backflow is limited to a (time dependent) subset of the open boundary, the velocity penalization methods appear to deliver better overall results in blood flow regime, while in air regime all methods perform satisfactorily, with a slight better performance obtained with the tangential regularization methods.

The results for each considered method are commented in more detail below.

- **Velocity penalization approach (without correction profile)**. This method achieved good results in presence of moderate backflow and recirculation in both hemodynamic and respiratory regimes. In fact, although the velocity penalization tends to flatten the incoming velocity profile, it induces only a minimal perturbation in the remaining (outflow) field, coherently with [2].
- **Velocity penalization approach (with correction profile)**. Including a correction profile (in the considered cases, based on a Stokes flow), the velocity penalization does not improve. In contrast, it becomes notably worse in blood flow regime, while it almost has not influence in air regime. However, it shall be observed that when the reference velocity is used within the velocity-penalization method, the approach is able to deliver very accurate results. Hence, it is to be expected that providing a better corrective profile would lead to more accurate results. On the other hand, in the presence of complex flows an assessment a priori of the profile shape could become prohibitive.
- **Velocity penalization + total pressure**. As observed in the first benchmark, the results obtained with this methods are very similar to the ones obtained with velocity penalization approach without correction profile.
- **Tangential derivative regularization**. The tangential regularization resulted the most accurate method in reproducing the pressure profile in both regimes, while being the second accurate for the velocity profile after velocity penalization methods. It shall be notice that, in blood regime, it yields to perturbations in the velocity profile also on the outflow part of the boundary, which might be due to the fact that this approach acts on the derivatives of the velocity.
- **Stokes-residual stabilization**. In air regime this method turn to give similar results than the tangential regularization, but the results appear to be affected by oscillations that affect the precision. In blood regime the tangential regularization clearly outperforms the Stokes-residual regularization, while in air regime the results are closer. This suggest the choice of the former one for open boundaries where local recirculation is expected.
- **Characteristics**. Although the method delivers stable results, the velocity field during backflow is affected by large errors, for both blood and air regimes.

6. CONCLUSIONS

This manuscript presents a detailed comparison of different strategies for the numerical solution of the incompressible Navier–Stokes Equations in presence of incoming flow (backflow) at open boundaries, with the particular focus on physiological flows. Although there have been recently several reports on this topic, reference problems for the assessment of stabilization methods are not available yet and comparisons of all (or at least most of) the treatments have been missing until the present work. Hence, the first goal of this study has been to construct suitable benchmark problems. In particular, we defined two different setups:

- *full backflow* (i.e., backflow over the entire open boundary), and
- *local backflow* (i.e., due to the convection of vortices downstream).

Since the main interest of the study lies in the numerical simulation of physiological flows, both blood- and airflow regimes for each of the benchmark setups have been considered. In the

DOI: 10.1002/cnm.2918

different cases, we generated a reference solution not affected by backflow instabilities, and we compared it against several formulations including backflow treatment.

This work considers several approaches reported in the literature (including stabilization techniques and the method of characteristics) and, up to date, it represents the most detailed and complete benchmarking available in this context. Moreover, the different methodologies have been briefly described, overviewing their main properties, in order to highlight the similarities and the main differences among the methods. The numerical results suggest that the most accurate methods in case of full reversal backflow are the ones based on penalization of the tangential derivatives, with a slight advantage for the Stokes-residual stabilization over the tangential regularization technique. This is consistent with comparisons presented in [7] for Womersley flows.

In the case with local backflow (i.e. with vortices), in blood flow regime the most accurate approaches are velocity penalization methods without any correction profile, since they affect mainly the regions with backflow leaving the outflow part rather unperturbed. In respiratory regime, all methods deliver satisfactory results, with a slight advantage of the tangential regularization. It is worth noticing that both the velocity penalization without corrective profile and the tangential regularization fit naturally within a finite element framework. These outcomes are part of the main results of this work, since detailed comparisons of these methods are not available in the literature.

The ultimate goal of this study is to set the basis for a *backflow-benchmark database*, with several test cases dedicated to backflow treatment. On the one hand, this will help the interested scientist to understand the different performances, in different settings, of the existing methods. On the other hand, this database will also provide the community with a set of tests for quickly assessing and comparing new proposed methods against the state of the art.

In line with this view, the considered approaches have been implemented in FreeFem++ [23] and all the data needed to carry out the simulation of the test problems (meshes – including mesh generator code –, boundary data, scripts) are available online. The restriction to 2D test cases can be considered one of the main limitation of this work. However, the extension to three-dimensional benchmarks will be considered, as well as the usage of other open source packages (e.g., Fenics [1]) are topics currently under consideration. By including new problems and new methods, the benchmark database will thus become a tool of utmost importance for the developments of numerical methods also in other fields of applications.

ACKNOWLEDGMENTS

The authors acknowledge Marc Thiriet for inspiring this benchmark study and to Celine Grandmont (INRIA Paris) for her excellent comments about the manuscript. Cristóbal Bertoglio thanks the funding of the Conicyt Basal Program PFB-03.

REFERENCES

1. M.S. Alnaes, J. Blechta, J. Hake, A. Johansson, B. Kehlet, A. Logg, C. Richardson, J. Ring, M. E. Rognes, and G. N. Wells, *The FEniCS Project Version 1.5*, Archive of Numerical Software **3** (2015).
2. Grégory Arbia, Irene Vignon-Clementel, T.-Y Hsia, and Jean-Frédéric Gerbeau, *Modified Navier-Stokes equations for the outflow boundary conditions in hemodynamics*, European Journal of Mechanics - B/Fluids **60** (2016), 175–188.
3. L. Baffico, C. Grandmont, and B. Maury, *Multiscale modeling of the respiratory tract.*, Models Methods Appl. Sci. **10** (2010), 59–93.
4. Y. Bazilevs, J.R. Gohean, T.J.R. Hughes, R.D. Moser, and Y. Zhang, *Patient-specific isogeometric fluid-structure interaction analysis of thoracic aortic blood flow due to implantation of the Jarvik 2000 left ventricular assist device*, Comput. Methods Appl. Mech. Engrg. **198** (2009), no. 45-46, 3534–3550.
5. Catherine Bègue, Carlos Conca, François Murat, and Olivier Pironneau, *A nouveau sur les équations de Stokes et de Navier-Stokes avec des conditions aux limites sur la pression*, Comptes rendus de l'Académie des sciences. Série 1, Mathématique **304** (1987), no. 1, 23–28.
6. C. Bertoglio and A. Caiazzo, *A tangential regularization method for backflow stabilization in hemodynamics*, J. Comp. Phys. **261** (2014), 162–171.

DOI: 10.1002/cnm.2918

7. ———, *A Stokes-residual backflow stabilization method applied to physiological flows*, J. Comp. Phys. **313** (2016), 260–278.
8. Cristóbal Bertoglio, *Forward and inverse problems in fluid-structure interaction. application to hemodynamics*, Ph.D. Thesis, Université Pierre et Marie Curie - Paris VI, November 2012.
9. O. Botella and R. Peyret, *Benchmark spectral results on the lid-driven cavity flow.*, Comput. Fluids **27** (1998), no. 4, 421–433 (English).
10. K Boukir, Y Maday, B Métivet, and E Razafindrakoto, *A high-order characteristics/finite element method for the incompressible navier-stokes equations*, International Journal for Numerical Methods in Fluids **25** (1997), no. 12, 1421–1454.
11. Franck Boyer and Pierre Fabrie, *Outflow boundary conditions for the incompressible non-homogeneous navier-stokes equations*, Discrete and Continuous Dynamical Systems-Series B **7** (2007), no. 2, pp–219.
12. M. Braack, *Outflow conditions for the Navier-Stokes equations with skew-symmetric formulation of the convective term*, Lecture Notes Comput. Science and Engineer., BAIL 2014 (P. Knobloch, ed.), vol. 108, Springer, 2016, pp. 35–45.
13. M. Braack and P.B. Mucha, *Directional do-nothing condition for the navier-stokes equations*, Journal of Computational Mathematics **32** (2014), no. 5, 507–521.
14. Ch.-H. Bruneau and P. Fabrie, *Effective downstream boundary conditions for incompressible Navier-Stokes equations*, International Journal for Numerical Methods in Fluids **19** (1994), no. 8, 693–705.
15. ———, *New effective boundary conditions for incompressible Navier-Stokes equations: a well-posedness result*, M2AN **30** (1996), no. 7, 815–840.
16. S. Dong, *An outflow boundary condition and algorithm for incompressible two-phase flows with phase field approach*, Journal of Computational Physics **266** (2014), 47–73.
17. S. Dong, G.E. Karniadakis, and C. Chrzssostomidis, *A robust and accurate outflow boundary condition for incompressible flow simulations on severely-truncated unbounded domains*, Journal of Computational Physics **261** (2014), 83–105.
18. M. Esmaily Moghadam, Y. Bazilevs, T.-Y. Hsia, I. Vignon-Clementel, A. Marsden, and Modeling of Congenital Hearts Alliance, *A comparison of outlet boundary treatments for prevention of backflow divergence with relevance to blood flow simulations*, Computational Mechanics **48** (2011), 277–291, 10.1007/s00466-011-0599-0.
19. Luca Formaggia, Alfio Quarteroni, and Christian Vergara, *On the physical consistency between three-dimensional and one-dimensional models in haemodynamics*, Journal of Computational Physics **244** (2013), 97–112.
20. Justine Fouchet-Incaux, *Artificial boundaries and formulations for the incompressible Navier-Stokes equations: applications to air and blood flows*, SeMA Journal **64** (2014), no. 1, 1–40.
21. U. Ghia, K.N. Ghia, and C.T. Shin, *High-Re solutions for incompressible flow using the Navier-Stokes equations and a multigrid method.*, J. Comput. Phys. **48** (1982), 387–411 (English).
22. V. Gravemeier, A. Comerford, L. Yoshihara, M. Ismail, and W.A. Wall, *A novel formulation for Neumann inflow boundary conditions in biomechanics*, International Journal for Numerical Methods in Biomedical Engineering **28** (2012), no. 5, 560–573.
23. F. Hecht, O. Pironneau, A. Le Hyaric, and K. Ohtsuka, *Freefem++ v. 2.11. user's manual*, University of Paris 6, 2010.
24. J.G. Heywood, R. Rannacher, and S. Turek, *Artificial boundaries and flux and pressure conditions for the incompressible Navier–Stokes equations*, International Journal for Numerical Methods in Fluids **22** (1996), 325–352.
25. Y. Huang and U. Ghia, *A multigrid method for solution of vorticity-velocity form of 3-D Navier- Stokes equations.*, Commun. Appl. Numer. Methods **8** (1992), no. 10, 707–719 (English).
26. M. Ismail, V. Gravemeier, A. Comerford, and W.A. Wall, *A stable approach for coupling multidimensional cardiovascular and pulmonary networks based on a novel pressure-flow rate or pressure-only neumann boundary condition formulation*, International Journal for Numerical Methods in Biomedical Engineering **30** (2014), no. 4, 447–469.
27. HJ Kim, CA Figueroa, TJR Hughes, KE Jansen, and CA Taylor, *Augmented lagrangian method for constraining the shape of velocity profiles at outlet boundaries for three-dimensional finite element simulations of blood flow*, Comp. Methods Appl. Mech. Engrg. **198** (2009), no. 45, 3551–3566.
28. Patrick Le Quéré, Catherine Weisman, Henri Paillère, Jan Vierendeels, Erik Dick, Roland Becker, Malte Braack, and James Locke, *Modelling of natural convection flows with large temperature differences: a benchmark problem for low mach number solvers. part 1. reference solutions*, ESAIM: Mathematical Modelling and Numerical Analysis **39** (2005), no. 3, 609–616.
29. J. Oakes, A. L. Marsden, C. Grandmont, C. Darquenne, and I. Vignon-Clementel, *Distribution of Aerosolized Particles in Healthy and Emphysematous Rat Lungs: Comparison Between Experimental and Numerical Studies*, Journal of Biomechanics **48** (2015), no. 6, 1147–1157.
30. J. Oakes, A. L. Marsden, C. Grandmont, S. C. Shadden, C. Darquenne, and I. Vignon-Clementel, *Airflow and Particle Deposition Simulations in Health and Emphysema: From In Vivo to In Silico Animal Experiments*, Annals of Biomedical Engineering **42** (2014), no. 4, 899–914.
31. O Pironneau and M Tabata, *Stability and convergence of a galerkin-characteristics finite element scheme of lumped mass type*, International Journal for Numerical Methods in Fluids **64** (2010), no. 10-12, 1240–1253.
32. Olivier Pironneau, *On the transport-diffusion algorithm and its applications to the navier-stokes equations*, Numerische Mathematik **38** (1982), no. 3, 309–332.
33. A. Porpora, P. Zunino, C. Vergara, and M. Piccinelli, *Numerical treatment of boundary conditions to replace lateral branches in hemodynamics*, International journal for numerical methods in biomedical engineering **28** (2012), no. 12, 1165–1183.

DOI: 10.1002/cnm.2918

34. Dong. S., *A convective-like energy-stable open boundary condition for simulations of incompressible flows*, J. Comp. Phys. **302** (2015), 300–328.
35. Michael Schäfer, Stefan Turek, Franz Durst, Egon Krause, and Rolf Rannacher, *Benchmark computations of laminar flow around a cylinder*, Springer, 1996.
36. Assia Soualah Alila, *Mathematical and numerical modelling of the humain lung*, Theses, Université Paris Sud - Paris XI, December 2007.
37. R. Temam, *Une méthode d'approximation de la solution des équations de Navier-Stokes*, Bull. Soc. Math. France **96** (1968), 115–152.

DOI: 10.1002/cnm.2918